# INELASTIC RESPONSE OF A BEAM SUBJECTED TO A COASTING LOAD

Thesis for the Degree of M. S. MICHIGAN STATE UNIVERSITY
F. FARHOOMAND
1968

LIBRARY
Michigan State
University







#### ABSTRACT

# INELASTIC RESPONSE OF A BEAM SUBJECTED TO A COASTING LOAD

#### by F. Farhoomand

In this thesis a numerical method for analyzing the dynamic response of a beam subjected to a coasting load is presented. The method is based on a discrete model with lumped mass and stiffness. The moment-curvature relation is of a general elastic-plastic-strain-hardening type with hysteretic behavior.

Numerical solutions are obtained using an iterative procedure for a simply-supported slender beam subjected to a coasting mass load.

The distinguishing feature of the present analysis lies in the treatment of the kinematics of the beam deformations. The analysis corresponds to a large-deflection theory.

In comparison with available experimental data, the present analytical results indicate a better agreement than those for the small-deflection analysis.

Certain parametric studies are also included in the thesis. It is found that for a load lighter than the ultimate load there exists a finite initial speed which is

most damaging to the beam. It is also found that a mass load heavier than the ultimate load can cross the beam, resulting in only moderate permanent deflections, if its initial speed is sufficiently large.

# INELASTIC RESPONSE OF A BEAM SUBJECTED TO A COASTING LOAD

Ву

#### F. Farhoomand

#### A THESIS

Submitted to
Michigan State University
in partial fulfillment of the requirements
for the degree of

MASTER OF SCIENCE

Department of Civil Engineering

6 49218

#### **ACKNOWLEDGMENTS**

The writer wishes to express his gratitude to his academic advisor, Dr. Robert K. Wen, Professor of Civil Engineering, whose advice proved to be invaluable. The writer is also indebted to Dr. Charles E. Cutts, Chairman of the Department of Civil Engineering, for his encouragement.

Sincere appreciation is extended to the National Science Foundation and to the Division of Engineering Research at Michigan State University, for their support of this investigation.

## TABLE OF CONTENTS

																	Page
ACKNO	OWLEDGI	MENTS		•			•	•			•	•		•	•	•	ii
LIST	OF FI	GURES		•		•	•	•	•		•	•	•	•	•	•	v
I.	INTR	ODUCT	ON	•		•	•	•	•		•	•	•	•	•	•	1
	1.2.	Gener Scope Nota	3														
II.	METH	OD OF	ANAI	LYS	IS	•		•	•		•	•	•	•	•	•	6
	2.2. 2.3.	Gener Discr Equat Jumps	cetiz tions	s 01	E Mo	otio	on		l A	cce	le:	rat	-ic	ons	5		
III.	METH	OD OF	NUME	ERIC	CAL	SOI	LUT	ION	Ī		•	•	•	•	•	•	17
	3.1.	Dimer	nsior cion	ıles	ss I	For	n o	f E	qu	ati	on	5 (	of				
		Desc:	cipti	l I	nte	grat					el	era	ati	.or	ıs		
		Nume: Mot	cical	L So	olut	tion	10	f E	qu	ati	on	s c	of				
		Use o		_													
IV.	COMP.	ARISON	• • •	ANA	· ·	FICA	AL A	ANE •	• E	XPE	RI	MEI	1T <i>P</i>	·	•	•	26
	4.2. 4.3.	Gener Mids Inter Perma	oan I	lve	For												
		Maxim				n De	efl	ect	io	n v	er	sus	3 5	Spe	eed	ī	

# Table of Contents (Continued)

	Page
V. INFLUENCE OF PARAMETERS	30
<ul><li>5.1. General</li><li>5.2. Influence of Load Weight</li><li>5.3. Influence of Beam Moment-Capacity</li></ul>	
VI. SUMMARY AND CONCLUSIONS	34
LIST OF REFERENCES	36
FIGURES	37
APPENDIXCOMPUTER PROGRAM	52

### LIST OF FIGURES

Figure		Page
1.	Initial State of Beam-Load System	37
2.	Moment-Curvature Diagram	38
3.	Free Body Diagrams	39
4.	Discrete Model	40
5.	Midspan Deflections versus Time	41
6.	Interactive Forces versus Time	43
7.	Permanent Sets	46
8.	Maximum Midspan Deflection versus Initial Speed (Analytical and Experimental)	47
9a.	Maximum Midspan Deflection versus Initial Speed (Effect of Load Weight)	48
9b.	Permanent Midspan Deflection versus Initial Speed (Effect of Load Weight)	49
10a.	Maximum Midspan Deflection versus Initial Speed (Effect of Beam Moment Capacity)	50
10b.	Permanent Midspan Deflection versus Initial Speed (Effect of Beam Moment Capacity)	51

#### I. INTRODUCTION

#### 1.1. General

In recent years the problem of moving loads on structures has been the subject of many theoretical and experimental investigations. Most of the works reported in the literature have been limited to the linearly elastic range of structural behavior. However, more recently there have been some studies that considered the inelastic range.

The history of past work in the latter category was reported in Ref. 5. In that reference was also presented a method of analyzing the dynamic inelastic response of beams subjected to moving loads. The method was based on a bilinear type of moment-curvature relation and a small-deflection approximation, i.e., the angle of the slope at any point of the beam was approximated by its sine.

The same problem was further considered in Ref. 3 in which both experimental and analytical results were presented. The analysis utilized the same approach as in Ref. 5 except that a more general type of moment-curvature relation was employed. Comparisons between the theoretical and experimental responses generally seemed satisfactory. However, serious discrepancies emerged near the end of crossings

for those cases in which the beam suffered appreciable permanent set. In such cases the analysis predicted a complete collapse of the beam while the experiments showed only a finite permanent set.

These discrepancies were reasoned to have resulted from the assumptions of the small deflection theory which led to two consequences: (1) the moving load maintained a constant horizontal speed and (2) the load effectively stayed on the beam over a longer period of time. Accordingly, it was felt that by using more exact geometrical relations in place of the small-deflection assumption it would be possible to improve on the theoretical analysis. This consideration, in fact, motivated the present work.

In passing it may be added that in recent years, the ultimate strength theory has been gaining increasing acceptance in structural engineering. However, comparative experimental and analytical works have been scarce in inelastic dynamics of structures. In this connection, the present study may have some value beyond its apparent scope of moving loads, as it also reflects the validity of the same general approach for other loading conditions.

#### 1.2. Scope

The physical system considered is first defined in Chapter 2. There the method of analysis, including the derivation of the equations of motion, is also presented. In

Chapter 3, the numerical method of solution is described.

Chapters 4 and 5 contain the numerical results of the study.

In Chapter 4, analytical results are compared with experimental ones. In Chapter 5, the influence of three important physical parameters on the response is studied. The last chapter comprises a summary of the present study.

### 1.3. Notation

The symbols and letters used in this report are listed in alphabetical order, with English letters preceding Greek letters. They are also defined where they are first introduced.

A letter with an upper bar represents a dimensionless variable. By the same token, a letter with one or two upper dots indicates a first or second derivative with respect to time.

 $a_1$ ,  $a_2$ ,  $a_3$  = auxiliary variables

A<sub>i</sub> = auxiliary variable

 $B_1$ ,  $B_2$ ,  $B_3$  = auxiliary variables

C = auxiliary variable

d<sub>i</sub> = auxiliary variable

dt = finite increment in time

E = modulus of elasticity

g = acceleration of gravity

h = length of panel

H; = X-component of internal force between joint (i) and panel (i) H<sub>i</sub> = X-component of internal force between joint (i) and panel (i-1)  $H_{\mathbf{i}}$ = auxiliary variable i, j = dummy subscripts = moment of inertia Ι k = subscript identifying the panel being traversed by load L = length of beam = lumped mass at any interior joint of m model = bending moment at joint (i)  $M_{i}$ Мy = yield moment; see Fig. 2 = number of panels = interactive force between load and Р model =  $4M_V/L$ ; yield load = total mass of beam  $Q_{b}$ QZ = mass of load t = time = time when load is passing joint (i) = time infinitesimally after t<sub>i</sub> = time infinitesimally before t;  $\mathbf{T}$ = fundamental period of elastic vibration

of beam

T <sub>s</sub>	= smallest period of elastic vibration
	of beam
v	= initial speed of load
$v_i^+$	= Y-component of internal force between
	joint (i) and panel (i)
v <sub>i</sub>	= Y-component of internal force between
	joint (i) and panel (i-1)
x	= X-coordinate of load
×i	= X-coordinate of joint (i)
X	= Cartesian coordinate
У	= Y-coordinate of load
Yi	= Y-coordinate of joint (i)
Y	= Cartesian coordinate
Δ	= $P_yL^3/(48EI)$ ; maximum elastic deflection
	of beam when $P_y$ is applied at midspan
$\phi_{ extbf{i}}$	= angle of relative rotation of two ad-
	jacent panels connected to joint (i)
$^{ heta}$ i	= angle of deviation of panel (i) from
_	X-axis

#### II. METHOD OF ANALYSIS

### 2.1. General

Consider a system of beam and load as shown in Fig. 1.

The beam is straight, slender and simply-supported. It has a uniform distribution of mass and stiffness. The left-hand support is hinged at the origin of the coordinate axes OX and OY. The right-hand support is allowed to slide along the X-axis.

The load consists of a single unsprung mass. It enters the beam at time t=0 with an initial speed v, and is to coast on the beam from the left to the right.

The relation between the bending moment and curvature of the beam is of the general elasto-inelastic type described in Ref. 3. Assuming a rectangular cross-section and referring to Fig. 2 the relation for loading is given by

$$M = EIk$$
 for  $k \le k_{y}$  (1a)

$$M = 1.5M_{v} - 0.5M_{v}(k_{v}/k)^{2}$$
 for  $k_{v} \le k \le 10k_{v}$  (1b)

$$M = 1.5M_{v} + 0.03EI(k - 10k_{v}) \text{ for } 10k_{v} \le k$$
 (1c)

where M denotes the bending moment, k the curvature, M the yield moment,  $k_y$  the yield curvature, E the modulus of

elasticity, and I the moment of inertia. The relations for unloading and reloading, after the initial elastic region is exceeded, depend on the history of deformation. They follow a hysteretic pattern as fully explained in Ref. 4.

The assumptions made in this study are outlined below.

- 1) Axial and shearing deformations are negligible.
- 2) Bending deformations are not affected by axial and shearing forces.
- 3) The beam has no rotary inertia.

### 2.2. Discretization of Beam

In order to accomplish a numerical analysis of the problem described in the preceding section, the continuous properties of the beam are lumped or discretized. The manner of discretization corresponds to that for "model B" discussed in Ref. 4. Accordingly, the beam is replaced by a finite number of massless rigid panels connected by flexible joints with lumped masses. The panels are further assumed to be of equal length h.

The lumped mass at any interior joint of the model is  $m = Q_b/n$ , where  $Q_b$  is the total mass of the beam and n the number of panels. Furthermore, at a boundary joint, the lumped mass is  $m/2 = Q_b/2n$ .

The moment-rotation relation for each interior joint (i) is obtained from Eqs. 1 by replacing M by  $M_{\hat{i}}$  and k by  $\phi_{\hat{i}}/h$ , where  $M_{\hat{i}}$  is the bending moment at joint (i) and  $\phi_{\hat{i}}$  the angle of relative rotation between panels (i-1) and (i).

## 2.3. Equations of Motion

Let k identify the panel being traversed by the coasting load at some typical instant t. Referring now to Fig. 3a, application of the linear momentum theorem to the coasting load yields

$$P \sin \theta_{k} = Q_{\chi} \ddot{x}$$
 (2)

and

$$Q_{\mathcal{I}}g - P \cos \theta_{\mathbf{k}} = Q_{\mathcal{I}}\ddot{y}$$
 (3)

in which P denotes the interactive force between the model and the moving load,  $\theta_k$  the angle of deviation of panel (k) from the X-axis,  $Q_l$  the mass of the load,  $(\ddot{x},\ddot{y})$  the acceleration components of the load, and g the acceleration of gravity.

Similarly, considering Fig. 3b, application of the linear momentum theorem to a generic panel (i) as well as to the specific panel (k) gives

$$H_{i+1}^{-} - H_{i}^{+} = 0$$
 where  $i \neq k$  (4a)

$$H_{k+1}^{-} - H_{k}^{+} - P \sin \theta_{k} = 0$$
 (4b)

and

$$V_{i+1}^{-} - V_{i}^{+} = 0 \quad \text{where } i \neq k$$
 (5a)

$$v_{k+1}^- - v_k^+ + P \cos \theta_k = 0$$
 (5b)

in which  $(H_i^+, V_i^+)$  and  $(H_i^-, V_i^-)$  are the internal forces acting on joint (i) transmitted by panels (i) and (i-1), respectively.

Another application of the same theorem to a generic joint (i) in Fig. 3c provides

$$H_{i}^{+} - H_{i}^{-} = m\ddot{x}_{i} \quad \text{where } i \neq n+1$$
 (6a)

$$H_{n+1}^+ - H_{n+1}^- = \frac{m}{2} \ddot{x}_{n+1}$$
 (6b)

and

$$v_i^+ - v_i^- = m\ddot{y}_i \tag{7}$$

where  $(\ddot{x}_i, \ddot{y}_i)$  denotes the acceleration components of joint (i).

Furthermore, application of the angular momentum theorem to the left end of a generic panel (i) as well as to the left end of the specific panel (k) gives

$$M_i - M_{i+1} - H_{i+1}$$
 h sin  $\theta_i + V_{i+1}$  h cos  $\theta_i = 0$  where  $i \neq k$  (8a)

$$M_k - M_{k+1} - H_{k+1} h \sin \theta_k + V_{k+1} h \cos \theta_k$$

$$+ P \frac{x - x_k}{\cos \theta_k} = 0$$
 (8b)

in which x and  $x_k$  are the X-coordinates of the load and joint (k), respectively.

To carry out an analysis of the system, Equations 1 through 8 must be supplemented by certain kinematical equations. These equations, with reference to Fig. 4, are readily given by

$$\theta_{i} = Arcsin \frac{y_{i+1} - y_{i}}{h}$$
 (9)

$$\phi_{i} = \theta_{i-1} - \theta_{i} \tag{10}$$

$$\mathbf{x}_{\mathbf{i}} = \mathbf{h} \sum_{\mathbf{j}=2}^{\mathbf{i}} \cos \theta_{\mathbf{j}-1} \tag{11}$$

$$y = y_k + (x - x_k) \tan \theta_k$$
 (12)

where (x,y) and  $(x_i,y_i)$  are the coordinates of the load and joint (i), respectively.

Taking the first partial derivative of Equations 11 and 12 with respect to time they are transformed into

$$\dot{\mathbf{x}}_{i} = -\frac{\dot{\mathbf{y}}_{i}}{\dot{\mathbf{y}}_{i}} (\dot{\mathbf{y}}_{j} - \dot{\mathbf{y}}_{j-1}) \tan \theta_{j-1}$$

$$\dot{\mathbf{y}} = \dot{\mathbf{y}}_{k} + (\dot{\mathbf{x}} - \dot{\mathbf{x}}_{k}) \tan \theta_{k} + \frac{(\mathbf{x} - \mathbf{x}_{k})(\dot{\mathbf{y}}_{k+1} - \dot{\mathbf{y}}_{k})}{h \cos^{3} \theta_{k}}$$

$$(13)$$

in which  $(\dot{x},\dot{y})$  and  $(\dot{x}_i,\dot{y}_i)$  are the velocity components of the load and joint (i), respectively.

Taking once more the first partial derivative of Equations 13 and 14 with respect to time they are further transformed into

$$\ddot{x}_{i} = -\frac{\dot{i}}{\dot{j}=2} \left( (\ddot{y}_{j} - \ddot{y}_{j-1}) \tan \theta_{j-1} + \frac{(\dot{y}_{j} - \dot{y}_{j-1})^{2}}{h \cos^{3} \theta_{j-1}} \right)$$

$$\ddot{y} = \ddot{y}_{k} + (\ddot{x} - \ddot{x}_{k}) \tan \theta_{k}$$

$$+ \frac{(x - x_{k}) (\ddot{y}_{k+1} - \ddot{y}_{k})}{h \cos^{3} \theta_{k}}$$

$$+ \frac{2(\dot{x} - \dot{x}_{k}) (\dot{y}_{k+1} - \dot{y}_{k})}{h \cos^{3} \theta_{k}}$$

$$+ \frac{3(x - x_{k}) (\dot{y}_{k+1} - \dot{y}_{k})^{2}}{h^{2} \cos^{4} \theta_{k}} \tan \theta_{k}$$

$$(16)$$

Elimination of  $\ddot{x}$  and  $\ddot{y}$  between Equations 2, 3 and 16 leads to the following equation for P.

$$P = Q_{l} \left( \frac{\mathbf{x} - \mathbf{x}_{k}}{\mathbf{h} \cos^{2} \theta_{k}} - \cos \theta_{k} \right) \ddot{\mathbf{y}}_{k}$$

$$- Q_{l} \frac{\mathbf{x} - \mathbf{x}_{k}}{\mathbf{h} \cos^{2} \theta_{k}} \ddot{\mathbf{y}}_{k+1} + Q_{l} \mathbf{g} \cos \theta_{k}$$

$$+ Q_{l} \ddot{\mathbf{x}}_{k} \sin \theta_{k} - 2Q_{l} \frac{(\dot{\mathbf{x}} - \dot{\mathbf{x}}_{k}) (\dot{\mathbf{y}}_{k+1} - \dot{\mathbf{y}}_{k})}{\mathbf{h} \cos^{2} \theta_{k}}$$

$$- 3Q_{l} \frac{(\mathbf{x} - \mathbf{x}_{k}) (\dot{\mathbf{y}}_{k+1} - \dot{\mathbf{y}}_{k})^{2}}{\mathbf{h}^{2} \cos^{3} \theta_{k}} \tan \theta_{k}$$

$$(17)$$

Elimination of  $H_{\dot{1}}^{\dot{1}}$  between Equations 4 and 6 leads to

$$H_{i}^{-} = -m\ddot{x}_{i} + H_{i+1}^{-}$$
 where  $i \neq k$ ,  $n + 1$  (18a)

$$H_{k}^{-} = -m\ddot{x}_{k} + H_{k+1}^{-} - P \sin \theta_{k}$$
 (18b)

$$H_{n+1}^{-} = -\frac{m}{2}\ddot{x}_{n+1} \tag{18c}$$

It should be recognized that in the above transition the boundary condition  $H_{n+1}^+ = 0$  has been used. Equations 18 are now solved for  $H_{i}^-$ .

$$H_{i}^{-} = -\frac{m}{2}\ddot{x}_{n+1} - m \sum_{j=i}^{n} \ddot{x}_{j} - P \sin \theta_{k} \text{ for } i \leq k$$
 (10a)

$$H_{i}^{-} = -\frac{m}{2}\ddot{x}_{n+1} - m \sum_{j=i}^{n} \ddot{x}_{j}$$
 for  $k < i \le n$  (19b)

$$H_{n+1}^{-} = -\frac{m}{2}\ddot{x}_{n+1}. \tag{19c}$$

For convenience in subsequent computations an auxiliary variable  $H_{\dot{1}}$  (which has no apparent physical meaning) is introduced.

$$H_{i} = -\frac{1}{2}\ddot{x}_{n+1} - \sum_{j=i}^{n} \ddot{x}_{j}$$
 (20)

Equations 19 are thus written as

$$H_{i}^{-} = mH_{i} - P \sin \theta_{k}$$
 for  $i \le k$  (21a)

$$H_{i}^{-} = mH_{i} \qquad \text{for } k < i \qquad (21b)$$

Solution of Equations 8 for  $V_{\dot{i}}^-$  with the latter substitution for  $H_{\dot{i}}^-$  yields

$$V_{i+1}^- = md_{i+1} - P \sin \theta_k \tan \theta_i$$
 for  $i < k$  (22a)

$$v_{k+1}^- = md_{k+1} - P \frac{x - x_k}{h \cos^2 \theta_k}$$
 (22b)

$$V_{i+1}^- = md_{i+1}$$
 for k < i (22c)

where

$$d_{i} = H_{i} \tan \theta_{i-1} + \frac{M_{i} - M_{i-1}}{mh \cos \theta_{i-1}}$$

Elimination of  $V_{i}^{\dagger}$  between Equations 5 and 7 yields

$$m\ddot{y}_{i} = V_{i+1}^{-} - V_{i}^{-} \quad \text{where } i \neq k$$
 (23a)

$$m\ddot{y}_{k} = V_{k+1}^{-} - V_{k}^{-} + P \cos \theta_{k}$$
 (23b)

Finally, substitution of Equations 22 into 23 gives the following differential equations of motion.

$$\ddot{y}_{i} = d_{i+1} - d_{i} - \frac{P}{m} \sin \theta_{k} (\tan \theta_{i} - \tan \theta_{i-1})$$

$$for i < k \qquad (24a)$$

$$\ddot{y}_{k} = d_{k+1} - d_{k} + \frac{P}{m} (\sin \theta_{k} \tan \theta_{k-1} + \cos \theta_{k} - \frac{x - x_{k}}{h \cos^{2} \theta_{k}})$$

$$(24b)$$

$$\ddot{y}_{k+1} = d_{k+2} - d_{k+1} + \frac{P}{m} \frac{x - x_k}{h \cos^2 \theta_k}$$
 (24c)

$$\ddot{y}_{i} = d_{i+1} - d_{i}$$
 for k+1 < i (24d)

# 2.4. Jumps in Velocities and Accelerations

It is evident that the velocity and acceleration of a mass load coasting on a smooth beam with continuous distribution of stiffness are continuous functions of time, so long as the load is in contact with the beam. However, if the discrete model used in the present analysis replaces the beam, these functions are no longer continuous. In fact, when the load is passing a joint, the velocity and acceleration of the load will experience sudden changes or "jumps." At the same time, similar jumps will also take place in the velocity and acceleration of the very joint being passed by the load.

#### 1) Jumps in Velocities

Let the time when the load is passing a joint (i) be denoted by  $t_i$ , and the instants immediately before and after that by  $t_i^-$  and  $t_i^+$ . Then, Equation 13 at times  $t_i^-$  and  $t_i^+$  becomes

$$\dot{x}_{i}^{-} = -(\dot{y}_{i}^{-} - \dot{y}_{i-1}) \tan \theta_{i-1} - \sum_{j=2}^{i-1} (\dot{y}_{j} - \dot{y}_{j-1}) \tan \theta_{j-1}$$

and

$$\dot{x}_{i}^{+} = -(\dot{y}_{i}^{+} - \dot{y}_{i-1}) \tan \theta_{i-1} - \sum_{j=2}^{i-1} (\dot{y}_{j} - \dot{y}_{j-1}) \tan \theta_{j-1}$$

in which the superscripts "-" and "+" refer, respectively, to  $t_i^-$  and  $t_i^+$ . Subtracting one of these two equations from the other, there results

$$\dot{x}_{i}^{+} = \dot{x}_{i}^{-} - (\dot{y}_{i}^{+} - \dot{y}_{i}^{-}) \tan \theta_{i-1}$$
 (25)

Letting  $x = x_i$  at time  $t_i^+$ , Equation 14 becomes

$$\dot{y}^{+} = (\dot{x}^{+} - \dot{x}_{i}^{-}) \tan \theta_{i} + \dot{y}_{i}^{+}$$
(26)

Furthermore, conservation of linear momentum in the X and Y directions provides

$$Q(\dot{x}^{+} - \dot{x}^{-}) + m(\dot{x}_{i}^{+} - \dot{x}_{i}^{-}) = 0$$
 (27)

and

$$Q(\dot{y}^{+} - \dot{y}^{-}) + m(\dot{y}_{i}^{+} - \dot{y}_{i}^{-}) = 0$$
 (28)

Elimination of  $\dot{x}^+$ ,  $\dot{y}^+$ , and  $\dot{x}_{\dot{1}}^+$  between Equations 25 through 28 produces

$$\dot{y}_{i}^{+} = \dot{y}_{i}^{-} + \frac{\dot{y}^{-} - \dot{y}_{i}^{-} - (\dot{x}^{-} - \dot{x}_{i}^{-}) \tan \theta_{i}}{(1 + \frac{m}{Q_{l}}) (1 + \tan \theta_{i} \tan \theta_{i-1})}$$
(29)

Next,  $\dot{x}_i^{\dagger}$  is determined by back substitution of  $\dot{y}_i^{\dagger}$  into Equation 25. Using  $\dot{x}_i^{\dagger}$  and  $\dot{y}_i^{\dagger}$ , Equations 27 and 28 yield  $\dot{x}^{\dagger}$  and  $\dot{y}^{\dagger}$ , respectively.

#### 2) Jumps in Accelerations

It is recalled that the interactive force between the load and the model is always normal to the panel being traversed by the load. Thus, in passing from  $t_{i}^{-}$  to  $t_{i}^{+}$ , the interactive force suddenly changes direction. This causes jumps in accelerations. However, all equations of kinetics must be satisfied. In order to account for these jumps, the transition from  $t_{i}^{-}$  to  $t_{i}^{+}$  is treated as a step in the general numerical integration procedure, to be discussed in the next chapter, with the following modifications:

(1) 
$$dt = t_i^+ - t_i^- = 0$$

(2) k is increased by one.

#### III. METHOD OF NUMERICAL SOLUTION

# 3.1. <u>Dimensionless Form of Equations</u> of Motion

In computing numerical results it is convenient to deal with dimensionless equations. To this end, the following dimensionless variables and parameters are introduced.

$$\overline{H}_{i} = \frac{h}{v^{2}}H_{i} \qquad \overline{M}_{i} = \frac{M_{i}}{M_{y}}$$

$$\overline{P} = \frac{P}{P_{y}} \qquad \overline{t} = \frac{v}{h}t$$

$$\overline{x} = \frac{x}{h} \qquad \overline{x} = \frac{\dot{x}}{v}$$

$$\overline{x} = \frac{h}{v^{2}}\ddot{x} \qquad \overline{y}_{i} = \frac{y_{i}}{h}$$

$$\dot{y}_{i} = \frac{\dot{y}_{i}}{v}$$

$$\alpha = \frac{v^{2}Q_{l}}{hP_{y}} \qquad \beta = \frac{gQ_{l}}{P_{y}}$$

$$\gamma = \frac{Q_{l}}{hM_{y}}$$

$$\gamma = \frac{EI}{hM_{y}}$$

where  $P_y = 4M_y/L$  denotes the "yield load."

With the use of the dimensionless variables and parameters, Equations 9, 10, 1, 15, 20, 17, 24, and 2 are, respectively cast in the following dimensionless form.

$$\theta_{i} = Arcsin (\bar{y}_{i+1} - \bar{y}_{i})$$
 (30)

$$\phi_{\mathbf{i}} = \theta_{\mathbf{i}-1} - \theta_{\mathbf{i}} \tag{31}$$

$$\overline{M}_{i} = \zeta \phi_{i}$$
 for  $\zeta \phi_{i} \leq 1$  (32a)

$$\overline{M}_{i} = 1.5 - 0.5(\zeta \phi_{i})^{-2}$$
 for  $1 \le \zeta \phi_{i} \le 10$  (32b)

$$\overline{M}_{i} = 1.5 + 0.03(\zeta \phi_{i} - 10)$$
 for  $10 \le \zeta \phi_{i}$  (32c)

$$\ddot{x}_{i} = -\sum_{j=2}^{i} \left( (\ddot{y}_{j} - \ddot{y}_{j-1}) \tan \theta_{j-1} + \frac{(\ddot{y}_{j} - \ddot{y}_{j-1})^{2}}{\cos^{3} \theta_{j-1}} \right)$$
(33)

$$\overline{H}_{i} = -\frac{1}{2}\ddot{x}_{n+1} - \sum_{j=i}^{n} \ddot{x}_{j}$$
 (34)

$$\overline{P} = B_1 \ddot{y}_k + B_2 \ddot{y}_{k+1} + B_3$$
 (35)

$$\ddot{\mathbf{y}}_{i} = \mathbf{A}_{i} + \mathbf{a}_{3}\overline{\mathbf{P}}$$
 for  $i < k$  (36a)

$$\ddot{\overline{y}}_{k} = A_{k} + a_{2}\overline{P} \tag{36b}$$

$$\ddot{\bar{y}}_{k+1} = A_{k+1} + A_1 \overline{P}$$
 (36c)

$$\ddot{\ddot{y}}_{i} = A_{i} \qquad \text{for } k + 1 < i \qquad (36d)$$

$$\ddot{\bar{\mathbf{x}}} = \frac{\bar{\mathbf{p}}}{\alpha} \sin \theta_{\mathbf{k}} \tag{37}$$

in which

$$B_{1} = \alpha \left( \frac{\bar{\mathbf{x}} - \bar{\mathbf{x}}_{k}}{\cos^{2} \theta_{k}} - \cos \theta_{k} \right)$$

$$B_{2} = -B_{1} - \alpha \cos \theta_{k}$$

$$B_{3} = \beta \cos \theta_{k} + \alpha \bar{\mathbf{x}}_{k} \sin \theta_{k}$$

$$-2\alpha \frac{(\dot{\bar{\mathbf{x}}} - \dot{\bar{\mathbf{x}}}_{k}) (\dot{\bar{\mathbf{y}}}_{k+1} - \dot{\bar{\mathbf{y}}}_{k})}{\cos^{2} \theta_{k}}$$

$$-3\alpha \frac{(\bar{\mathbf{x}} - \bar{\mathbf{x}}_{k}) (\dot{\bar{\mathbf{y}}}_{k+1} - \dot{\bar{\mathbf{y}}}_{k})^{2}}{\cos^{3} \theta_{k}} \tan \theta_{k}$$

$$A_{i} = \bar{H}_{i+1} \tan \theta_{i} - \bar{H}_{i} \tan \theta_{i-1}$$

$$+ \frac{\gamma n^{2}}{4\alpha} \left( \frac{\bar{M}_{i+1} - \bar{M}_{i}}{\cos \theta_{i}} - \frac{\bar{M}_{i} - \bar{M}_{i-1}}{\cos \theta_{i-1}} \right)$$

$$a_{1} = \frac{\gamma n}{\alpha} \frac{\bar{\mathbf{x}} - \bar{\mathbf{x}}_{k}}{\cos^{2} \theta_{k}}$$

$$a_{2} = \frac{\gamma n}{\alpha} (\sin \theta_{k} \tan \theta_{k-1} + \cos \theta_{k}) - a_{1}$$

For completeness, Equations 29, 25, 28, and 27 are also put in the following dimensionless form.

 $a_3 = -\frac{\gamma n}{\alpha} \sin \theta_k (\tan \theta_i - \tan \theta_{i-1})$ 

#### III. METHOD OF NUMERICAL SOLUTION

# 3.1. <u>Dimensionless Form of Equations</u> of Motion

In computing numerical results it is convenient to deal with dimensionless equations. To this end, the following dimensionless variables and parameters are introduced.

$$\overline{H}_{i} = \frac{h}{v^{2}}H_{i} \qquad \overline{M}_{i} = \frac{M_{i}}{M_{y}}$$

$$\overline{P} = \frac{P}{P_{y}} \qquad \overline{t} = \frac{V}{h}t$$

$$\overline{x} = \frac{x}{h} \qquad \overline{x} = \frac{\dot{x}}{v}$$

$$\overline{x} = \frac{h}{v^{2}}\ddot{x} \qquad \overline{y}_{i} = \frac{Y_{i}}{h}$$

$$\dot{y}_{i} = \frac{\dot{y}_{i}}{v} \qquad \overline{y}_{i} = \frac{h}{v^{2}}\ddot{y}_{i}$$

$$\alpha = \frac{v^{2}Q_{l}}{hP_{y}} \qquad \beta = \frac{gQ_{l}}{P_{y}}$$

$$\gamma = \frac{Q_{l}}{Q_{h}} \qquad \zeta = \frac{EI}{hM_{y}}$$

where  $P_y = 4M_y/L$  denotes the "yield load."

With the use of the dimensionless variables and parameters, Equations 9, 10, 1, 15, 20, 17, 24, and 2 are, respectively cast in the following dimensionless form.

$$\theta_{i} = Arcsin (\bar{y}_{i+1} - \bar{y}_{i})$$
 (30)

$$\phi_{i} = \theta_{i-1} - \theta_{i} \tag{31}$$

$$\overline{M}_{i} = \zeta \phi_{i}$$
 for  $\zeta \phi_{i} \leq 1$  (32a)

$$\overline{M}_{i} = 1.5 - 0.5(\zeta \phi_{i})^{-2}$$
 for  $1 \le \zeta \phi_{i} \le 10$  (32b)

$$\overline{M}_{i} = 1.5 + 0.03(\zeta \phi_{i} - 10)$$
 for  $10 \le \zeta \phi_{i}$  (32c)

$$\ddot{\ddot{x}}_{i} = -\sum_{j=2}^{i} \left( (\ddot{\ddot{y}}_{j} - \ddot{\ddot{y}}_{j-1}) \tan \theta_{j-1} + \frac{(\ddot{\ddot{y}}_{j} - \ddot{\ddot{y}}_{j-1})^{2}}{\cos^{3} \theta_{j-1}} \right)$$
(33)

$$\overline{H}_{i} = -\frac{1}{2}\ddot{x}_{n+1} - \sum_{j=i}^{n} \ddot{x}_{j}$$
 (34)

$$\overline{P} = B_1 \ddot{\overline{y}}_k + B_2 \ddot{\overline{y}}_{k+1} + B_3$$
 (35)

$$\ddot{\ddot{y}}_{i} = A_{i} + a_{3}\overline{P} \qquad \text{for } i < k \qquad (36a)$$

$$\ddot{\overline{y}}_{k} = A_{k} + a_{2}\overline{P} \tag{36b}$$

$$\ddot{\ddot{y}}_{k+1} = A_{k+1} + a_1 \overline{P} \tag{36c}$$

$$\ddot{\ddot{y}}_{i} = A_{i} \qquad \text{for } k + 1 < i \qquad (36d)$$

$$\ddot{\ddot{\mathbf{x}}} = \frac{\overline{\mathbf{p}}}{\alpha} \sin \theta_{\mathbf{k}} \tag{37}$$

in which

$$B_{1} = \alpha \left( \frac{\bar{\mathbf{x}} - \bar{\mathbf{x}}_{k}}{\cos^{2} \theta_{k}} - \cos \theta_{k} \right)$$

$$B_{2} = -B_{1} - \alpha \cos \theta_{k}$$

$$B_{3} = \beta \cos \theta_{k} + \alpha \bar{\mathbf{x}}_{k} \sin \theta_{k}$$

$$-2\alpha \frac{(\bar{\mathbf{x}} - \bar{\mathbf{x}}_{k})(\bar{\mathbf{y}}_{k+1} - \bar{\mathbf{y}}_{k})}{\cos^{2} \theta_{k}}$$

$$-3\alpha \frac{(\bar{\mathbf{x}} - \bar{\mathbf{x}}_{k})(\bar{\mathbf{y}}_{k+1} - \bar{\mathbf{y}}_{k})^{2}}{\cos^{3} \theta_{k}} \tan \theta_{k}$$

$$A_{i} = \bar{H}_{i+1} \tan \theta_{i} - \bar{H}_{i} \tan \theta_{i-1}$$

$$+ \frac{\gamma n^{2}}{4\alpha} \left( \frac{\bar{M}_{i+1} - \bar{M}_{i}}{\cos \theta_{i}} - \frac{\bar{M}_{i} - \bar{M}_{i-1}}{\cos \theta_{i-1}} \right)$$

$$a_{1} = \frac{\gamma n}{\alpha} \frac{\bar{\mathbf{x}} - \bar{\mathbf{x}}_{k}}{\cos^{2} \theta_{k}}$$

For completeness, Equations 29, 25, 28, and 27 are also put in the following dimensionless form.

 $a_2 = \frac{\gamma n}{\alpha} (\sin \theta_k \tan \theta_{k-1} + \cos \theta_k) - a_1$ 

 $a_3 = -\frac{\gamma n}{\alpha} \sin \theta_k (\tan \theta_i - \tan \theta_{i-1})$ 

$$\dot{\bar{y}}_{i}^{+} = \dot{\bar{y}}_{i}^{-} + \gamma n \frac{\dot{\bar{y}}^{-} - \dot{\bar{y}}_{i}^{-} - (\dot{\bar{x}}^{-} - \dot{\bar{x}}_{i}^{-}) \tan \theta_{i}}{(1 + \gamma n) (1 + \tan \theta_{i} \tan \theta_{i-1})}$$
(38)

$$\dot{\bar{\mathbf{x}}}_{i}^{+} = \dot{\bar{\mathbf{x}}}_{i}^{-} - (\dot{\bar{\mathbf{y}}}_{i}^{+} - \dot{\bar{\mathbf{y}}}_{i}^{-}) \quad \tan \theta_{i-1}$$
 (39)

$$\dot{\bar{y}}^{+} = \dot{\bar{y}}^{-} - \frac{\dot{\bar{y}}_{\dot{1}}^{+} - \dot{\bar{y}}_{\dot{1}}^{-}}{\gamma n} \tag{40}$$

$$\dot{\bar{x}}^{+} = \dot{\bar{x}}^{-} - \frac{\dot{\bar{x}}_{1}^{+} - \dot{\bar{x}}_{1}^{-}}{\gamma n} \tag{41}$$

### 3.2. Description of Parameters

The problem under consideration has eight dimensional physical parameters: n, L,  $Q_b$ , EI,  $M_y$ , v,  $Q_l$ , and g. According to the theory of dimensional analysis these can be grouped into five independent dimensionless parameters which may be chosen to be n,  $\alpha$ ,  $\beta$ ,  $\gamma$ , and  $\zeta$ , as listed in the preceding section. Alternatively, any other independent combination of these parameters can be adopted.

the interest to interpret the physical character of the parameters  $\alpha$ ,  $\beta$ ,  $\gamma$ , and  $\zeta$ . The speed parameter  $\alpha = v^2 Q_{\tilde{l}}/h P_{\tilde{l}}$  is directly proportional to the initial kinetic energy of the load. The weight parameter  $\beta = g Q_{\tilde{l}}/P_{\tilde{l}}$  is a measure of the load weight in terms of the yield load. The mass parameter  $\gamma = Q_{\tilde{l}}/Q_{\tilde{b}}$  stands for the ratio of the load mass to the beam mass. The stiffness parameter  $\zeta = EI/h M_{\tilde{l}}$  is such that its reciprocal represents the angle of rotation  $\phi_{\tilde{l}}$  when  $M_{\tilde{l}} = M_{\tilde{l}}$ .

# 3.3. <u>Numerical Integration of Accelerations</u> and Velocities

In order to integrate the accelerations and velocities numerically, the so-called  $\beta$  method of integration as outlined in Ref. 2, with  $\beta$  = 0, is used.

Introducing  $d\overline{t}$  to denote a small increment in  $\overline{t}$  , the formulas for integrating  $\ddot{\overline{x}}$  and  $\dot{\overline{x}}$  are

$$\dot{\bar{x}}(\bar{t} + d\bar{t}) = \dot{\bar{x}}(\bar{t}) + 0.5 \left( \ddot{\bar{x}}(\bar{t}) + \ddot{\bar{x}}(\bar{t} + d\bar{t}) \right) d\bar{t}$$
 (42a)

$$\bar{x}(\bar{t} + d\bar{t}) = \bar{x}(\bar{t}) + \dot{\bar{x}}(\bar{t})d\bar{t} + 0.5\dot{\bar{x}}(\bar{t})d\bar{t}^2 \qquad (42b)$$

Similarly for  $\ddot{\ddot{y}}_{i}$  and  $\dot{\ddot{\ddot{y}}}_{i}$ , they are

$$\dot{\bar{y}}_{i}(\bar{t} + d\bar{t}) = \dot{\bar{y}}_{i}(\bar{t}) + 0.5(\ddot{\bar{y}}_{i}(\bar{t}) + \ddot{\bar{y}}_{i}(\bar{t} + d\bar{t}))d\bar{t}$$
(43a)

$$\bar{y}_{i}(\bar{t} + d\bar{t}) = \bar{y}_{i}(\bar{t}) + \hat{y}_{i}(\bar{t})d\bar{t} + 0.5\ddot{y}_{i}(\bar{t})d\bar{t}^{2}$$
 (43b)

The truncation error of these formulas is  $0(d\bar{t}^3)$ .

According to Ref. 2, in order to assure stability of the integration procedure, the dimensional time increment dt for each step must be less than  $1/\pi$  times  $T_s$ , the smallest period of elastic vibration of the beam. In this case  $T_s = T/n^2$ , where T is the fundamental period of vibration of the beam and n the number of panels into which the beam is divided.

# 3.4. Numerical Solution of Equations of Motion

Equations 36 and 37 constitute the governing equations of motion. Since these differential equations are nonlinear and heavily coupled, a closed-form solution is practically impossible. Furthermore, it does not even seem feasible to obtain a direct numerical solution (by using the integration formulas: Equations 42 and 43). Thus, it appears that iterative methods are the only alternatives.

Among various possibilities, the following procedure seems to be most expeditious. Assuming a set of values for  $\ddot{x}(\bar{t}+d\bar{t})$  and  $\ddot{y}_{i}(\bar{t}+d\bar{t})$  and using Equations 42 and 43,  $\dot{\bar{x}}$ ,  $\ddot{x}$ ,  $\dot{\bar{y}}_{i}$ , and  $\ddot{y}_{i}$ , at time  $\bar{t}+d\bar{t}$ , are computed. Then, Equations 30 through 35 are used to compute  $\theta_{i}$ ,  $\overline{M}_{i}$ ,  $\overline{H}_{i}$ , and  $\overline{P}$ . These values are now substituted into Equations 36 and 37 to obtain a new set of values for  $\ddot{\bar{x}}(\bar{t}+d\bar{t})$  and  $\ddot{\bar{y}}_{i}(\bar{t}+d\bar{t})$  which, of course, is to be compared with the assumed set.

The above procedure turned out to be divergent. Several other procedures were tried based on different sequences of substitutions of the variables and/or different forms of the equations modified by substitutions of the variables. Divergence ensued in all these attempts before the following successful procedure was found.

The procedure requires a recast of the governing equations. Replacing  $\overline{P}$  in Equations 36 by Equation 35, the former equations are transformed into the following.

$$\ddot{y}_{i} = A_{i} + a_{3}(B_{1}\ddot{y}_{k} + B_{2}\ddot{y}_{k+1} + B_{3})$$
 for  $i < k$  (44a)

$$\ddot{\bar{y}}_{k} = A_{k} + a_{2}(B_{1}\ddot{\bar{y}}_{k} + B_{2}\ddot{\bar{y}}_{k+1} + B_{3})$$
 (44b)

$$\ddot{\bar{y}}_{k+1} = A_{k+1} + a_1 (B_1 \ddot{\bar{y}}_k + B_2 \ddot{\bar{y}}_{k+1} + B_3)$$
 (44c)

$$\ddot{\bar{y}}_{i} = A_{i} \qquad \text{for } k+1 < i \quad (44d)$$

Regarding Equations 44b and c as two linear equations with two unknowns  $\ddot{\ddot{y}}_k$  and  $\ddot{\ddot{y}}_{k+1}$ , they are solved by Cramer's rule. Thus,  $\ddot{\ddot{y}}_k$  and  $\ddot{\ddot{y}}_{k+1}$  are given by

$$\ddot{\ddot{y}}_{k} = A_{k} + a_{2}C \tag{45b}$$

$$\ddot{\ddot{y}}_{k+1} = A_{k+1} + a_1^C$$
 (45c)

where

$$C = \frac{B_1 A_k + B_2 A_{k+1} + B_3}{1 - a_1 B_2 - a_2 B_1}$$

It must be noted that in the transition from Equations 44b, c to Equations 45 b, c, the auxiliary variables  $^{A}_{k}$ ,  $^{A}_{k+1}$ , and  $^{B}_{3}$  are treated as constants although they include  $\ddot{\bar{y}}_{k}$  and  $\ddot{\bar{y}}_{k+1}$  implicitly.

The next step is to substitute  $\ddot{y}_k$  and  $\ddot{y}_{k+1}$  from Equations 45b, c into Equation 44a. The resulting equation along with Equations 45b, c and 44d constitute the desired form of the equations of motion. For future reference, they are grouped in the following.

$$\ddot{\ddot{y}}_i = A_i + a_3 C \qquad \text{for } i < k \qquad (45a)$$

$$\ddot{\ddot{y}}_{k} = A_{k} + a_{2}C \tag{45b}$$

$$\ddot{\ddot{y}}_{k+1} = A_{k+1} + a_1 C$$
 (45c)

$$\ddot{\overline{y}}_{i} = A_{i} \qquad \text{for } k + 1 < i \quad (45d)$$

It is now shown how a step-by-step numerical solution of the equations of motion is performed.

- 1) At time  $\bar{t}$ , the beginning of an arbitrary step,  $\ddot{\bar{x}}(\bar{t})$ ,  $\dot{\bar{x}}(\bar{t})$ ,  $x(\bar{t})$ , and  $\ddot{\bar{y}}_{i}(\bar{t})$ ,  $\dot{\bar{y}}_{i}(\bar{t})$ ,  $\bar{y}_{i}(\bar{t})$  are known.
- 2) In order to have the iteration started, the unknowns  $\ddot{x}(\bar{t}+d\bar{t}) \ddot{\ddot{y}}_{i}(\bar{t}+d\bar{t})$  are set equal to  $\ddot{\ddot{x}}(\bar{t})$  and  $\ddot{\ddot{y}}_{i}(\bar{t})$ , respectively. Using Equations 42,  $\dot{\ddot{x}}(\bar{t}+d\bar{t})$  and  $\ddot{x}(\bar{t}+d\bar{t})$  are computed.
- 3) Having the assumed values for  $\ddot{\bar{y}}_i(\bar{t}+d\bar{t})$ , Equations 43 are used to compute  $\dot{\bar{y}}_i(\bar{t}+d\bar{t})$  and  $\bar{y}_i(\bar{t}+d\bar{t})$ .
- 4) The variables  $\theta_i$ ,  $\overline{M}_i$ , and  $\overline{H}_i$  are now computed by making use of Equations 30 through 34. Next, the auxiliary variables  $a_1$ ,  $a_2$ ,  $a_3$ ,  $A_j$ ,  $B_1$ ,  $B_2$ ,  $B_3$ , and C are computed.
- 5) Equations 45 readily produce new values for  $\ddot{y}_i(\bar{t} + d\bar{t})$  which are compared with the assumed ones used in part 3 to see whether their differences are within an allowable tolerance.
- 6a) If not, the newly computed  $\ddot{y}_i(\bar{t}+d\bar{t})$  are used as assumed  $\ddot{y}_i(\bar{t}+d\bar{t})$  in part 3 to start another cycle of iteration.

- 6b) If yes, the iteration is said to have converged.
- 7) By means of Equations 37 and 42,  $\ddot{\bar{x}}(\bar{t} + d\bar{t})$ ,  $\dot{\bar{x}}(\bar{t} + d\bar{t})$ , and  $\bar{x}(\bar{t} + d\bar{t})$  are successively computed to complete the necessary initial conditions for the next time interval of the integration.

In conclusion, it is worth observing that  $\ddot{\bar{x}}$  is not involved in the iterations. The reason is that  $\ddot{\bar{x}}$  is always relatively small compared to  $\ddot{\bar{y}}_i$ . It is, however, possible to include  $\ddot{\bar{x}}$  in the iterations. In fact, this was carried out in several solutions. The results appeared to be practically the same as those obtained without this refinement.

# 3.5. <u>Use of Computer</u>

The numerical results presented in the next two chapters were obtained on the CDC3600 digital computer of Michigan State University. A copy of the FORTRAN program, and the formats of the parameters as well as some other pertinent details are compiled in the Appendix.

# IV. COMPARISON OF ANALYTICAL AND EXPERIMENTAL RESULTS

#### 4.1. General

This chapter is devoted to comparing certain numerical results obtained from: (1) the present large-deflection analysis, (2) the laboratory experiments, and (3) the small-deflection analysis. The experimental data are taken from Ref. 3. The experimental set-up is briefly described below.

The beams used were made of mild steel. They were rectangular in cross section and had the following average properties: weight = 1.97 lb.; length = 24 in.; modulus of section = 0.0104 cu. in.; static yield stress = 30,300 psi; modulus of elasticity = 28,000,000 psi.

The loads used weighed in the neighborhood of 70 lb. Their initial speeds varied from approximately 6 to 20 fps.

It may be recalled that the following simplifying assumptions made in the small-deflection theory have been removed in the present large-deflection analysis: (1) the angle of the slope at any point of the beam is equal to its sine, and (2) the speed of the load is constant.

In both analyses to account for the dynamic nature of the loading, the yield stress is computed by multiplying

the static yield stress by a factor of  $1 + (0.0004/t_d)^{1/6}$ , where  $t_d$  is the time needed to initiate plastic deformation. According to Ref. 3, the time  $t_d$ , which must be less than L/v, is chosen to be (L/v)/3.

## 4.2. Midspan Deflection versus Time

Figures 5a, b, c illustrate the midspan deflection versus time for three initial speeds, 6.56, 11.30 and 13.50 fps. From Fig. 5a, it is seen that for the low speed, 6.56 fps., a fairly good agreement exists between either analytical graph and the experimental one.

For the higher speeds, 11.30 and 13.50 fps., Figs. 5b, c show that the experimental and analytical midspan deflections stayed close to one another until 90% of the beam had been traversed by the load. There the graph associated with the large-deflection theory still followed the experimental graph and they both rebounded. On the other hand, the deflection predicted by the small-deflection theory continued to increase, indicating a collapse of the beam, which of course did not take place in the experiments.

#### 4.3. Interactive Force versus Time

For the same initial speeds, Figs. 6a, b, c illustrate the interactive force versus time. These figures reveal the fact that the graphs generated by the two versions of analyses differ only slightly. For the low speed they also follow the experimental graph during the entire

passage of the load on the beam. But, for each one of the higher speeds, the analytical and experimental graphs begin to diverge after the load has traversed 90% of the beam. In fact, both analytical interactive forces become much larger than that of the experiments.

#### 4.4. Permanent Sets

For the low speed, 6.56 fps., there was no measurable permanent set in the experiments, and analytically the set was negligibly small. For the higher speeds, 11.30 and 13.50 fps., the permanent sets are presented in Figs. 7a, b. It should be noted that in each figure the graph corresponding to the large-deflection theory is plotted with the same scale as that for the experimental data. However, a scale of an order of magnitude smaller is used in plotting the graph associated with the small-deflection theory.

It is seen that the graphs generated by the small-deflection analysis neither in magnitude, nor in overall shape, agree with the experimental graphs. Indeed, the magnitudes differ by a factor of approximately 10. On the other hand, the shape of the damaged beams predicted by the large-deflection theory agree quite well with the experimental data. The difference in magnitudes is still large, that is, 100% to 250%. However, they do represent an improvement over the small-deflection theory. In view of the fact that the present problem involves unconstrained plasticity, a discrepancy of order of 100% or so between

the analytical and experimental results might be considered as not excessive.

# 4.5. Maximum Midspan Deflection versus Speed

For the last stage of comparison, the maximum midspan deflection of the beam is plotted in Fig. 8 against the initial speed of the load. The analytical graphs obtained for  $\beta=0.9$  and 1.3 are compared with the experimental data taken from Ref. 1. It is observed that for the lighter load ( $\beta=0.9$ ) the relevant graphs are almost coincident. For the heavier load ( $\beta=1.3$ ), they differ by approximately 20% although their overall shapes are harmonious. Thus, on this item of comparison, the results based on the largedeflection theory and experiments also appear to agree well.

#### V. INFLUENCE OF PARAMETERS

# 5.1. General

In order to gain some insight into the physics of the problem, the effects of the initial speed of the load on the midspan deflection of the beam are considered. Moreover, these effects are studied for loads of different weights and also for beams of different moment capacities.

#### 5.2. Influence of Load Weight

In Figs. 9a, b are presented, respectively, the maximum midspan deflection and permanent set for a range of v varying from  $0.5\sqrt{hg}$  to  $16\sqrt{hg}$ . In each figure three graphs are plotted which correspond to  $\beta=0.9$ , 1.3, 1.7, and the following parameters: n=10,  $\gamma/\beta=1$ , and  $\zeta=50$ . These data may be regarded as representing a bridge with L=40 ft.,  $EI=2\times10^8$  lb. ft.<sup>2</sup>,  $M_{\gamma}=10^6$  lb. ft.,  $gQ_b=10^5$  lb., and three loads with  $gQ_{\chi}=0.9\times10^5$ , 1.3  $\times10^5$ , 1.7  $\times10^5$  lb., v=5.67 to 181.44 fps.

Fig. 9a shows that all the graphs have the same general trend. The maximum midspan deflections increase with the initial speed of the load, rising to a peak and gradually tapering off at higher speeds. They are also

seen to be larger for heavier loads. The deflections at the peaks are  $8.10\Delta$ ,  $4.35\Delta$ , and  $2.17\Delta$  for  $\beta$  = 1.7, 1.3, and 0.9, respectively.

To explain qualitatively the relative positions of the peaks on the speed axis, the beam-load system might be considered as having a single degree of freedom. Considering the load to be situated at the midspan of the beam, the fundamental circular frequency of the system (assumed elastic) is readily given by  $\sqrt{96\text{EIL}^{-3}/(2Q_l+Q_b)}$ . The circular frequency of the "forcing function" due to the moving load may be approximated by  $\pi v/L$ . These two frequencies are equated, from which the "resonant speed" is found to be  $\sqrt{24\pi^{-2}\zeta\gamma\beta^{-1}/(2\gamma+1)}$ .  $\sqrt{\text{hg}}$ . Accordingly, the resonant speeds pertaining to the data in Fig. 9a are  $5.26\sqrt{\text{hg}}$ ,  $5.81\sqrt{\text{hg}}$ , and  $6.59\sqrt{\text{hg}}$ , for  $\beta=1.7$ , 1.3, and 0.9, respectively.

These estimated resonant speeds are to be compared with  $2.10\sqrt{hg}$ ,  $3.40\sqrt{hg}$ , and  $5.70\sqrt{hg}$  which correspond to the peaks of the graphs in Fig. 9a. Qualitatively, the agreement is fairly good inspite of the fact that the model used in the estimation is a very rough one for the actual system. This comparison means that the system appeared to have responded like one with a single degree of freedom.

The graphs of permanent sets shown in Fig. 9b also exhibit the same general features as in Fig. 9a.

## 5.3. Influence of Beam Moment-Capacity

In Figs. 10a, b are presented six graphs similar to those shown previously in Figs. 9a, b. The three graphs of each figure correspond to  $\beta=1.0$ , 1.5, 2.0 and the following parameters: n=10,  $\gamma=1.5$ ,  $\zeta/\beta=50$ . With this choice of parameters, M is the only physical parameter which is variable between the three graphs.

Fig. 10a exhibits essentially the same characteristics as those shown in Fig. 9a except for the graph corresponding to  $\beta=2.0$ . For the range of v considered, this graph does not rise to any peak. In other words, the maximum midspan deflection increases steadily as v decreases. This is explained in the following by referring to the stiffness properties of the beam.

For  $\beta$  = 1.5, when v approaches zero the fully plastic moment (1.5M<sub>y</sub>) will be reached at the midspan, but the beam will not collapse because of the strain-hardening properties. The stiffness in the strain-hardening region is, however, very small (3% of the initial elastic stiffness). Therefore, the beam is expected to collapse only when  $\beta$  is larger than 1.5 and v approaches zero.

For  $\beta$  = 1.5 and 1.0 each graph attains a peak. It is possible to explain the relative positions of these peaks on the speed axis on a basis similar to that discussed previously in connection with the peaks in Fig. 9a. However, in this case since EI, L,  $Q_b$ , and  $Q_L$  are the same, the

natural frequency of the beam-load system may be regarded as depending on the "effective stiffness" of the beam. For any joint (i), the effective stiffness may be considered to be equal to the value of M divided by the maximum value of  $\phi_i$  that has incurred. Since this maximum is obviously smaller for the beam with  $\beta=1.0$  than for the one with  $\beta=1.5$ , the load-beam system corresponding to  $\beta=1.0$  is stiffer and would have a higher "natural frequency." It follows that the peak for  $\beta=1.0$  graph should take place at a higher frequency of the forcing function, that is, at a higher initial speed of the load.

The graphs of permanent sets illustrated in Fig. 10b also indicate the same trends as in Fig. 10a discussed in the preceding.

#### VI. SUMMARY AND CONCLUSIONS

A numerical method for analyzing the dynamic response of a beam subjected to a coasting mass load was presented. The method was based on a discrete model with lumped mass and stiffness. In defining the stiffness properties of the beam, the type of elastic-plastic-strain-hardening and hysteretic behavior of such material as mild steel was considered.

A similar method of analysis had been reported in Ref. 3. The present method differs from that in the treatment of the kinematics of the problem. While the work of Ref. 3 may be called a small-deflection theory, the present method represents a large-deflection analysis.

In comparison with experimental data (Ref. 3) the present analytical results indicate better agreements than those of the small-deflection theory. This is particularly true for the cases in which large permanent deflections have taken place. Since in solving such problems the occurrence of large permanent deflections is in general not always predictable, it is safer to use the large-deflection analysis.

Certain parametric studies, considering the influence of initial load speed, load weight, and beam yield-moment,

were also included in this report. For the range of parameters considered the following were found to be noteworthy.

- 1) As long as the load weight was less than the static ultimate load (1.5P<sub>y</sub>) the response (maximum or permanent midspan deflection) showed a relative maximum when plotted against the initial speed of the load. In other words, this relative maximum occurred at a "most damaging" initial speed.
- 2) When the load weight was greater than the static ultimate load, no relative maximum was obtained. Instead,
  the response continued to increase as the initial speed
  of the load decreased. However, such heavy loads could
  still cross the beam, with only moderate permanent deflections, if their initial speeds were sufficiently
  large.
- 3) In connection with the relative maxima, the behavior of the system could be qualitatively explained on the basis of a single-degree-of-freedom system. In this system the load played the role of the forcing function and, in part, also that of the mass. The beam mainly supplied the stiffness, although its contribution to the mass was also substantial.
- 4) The effect of an increase in the load weight was qualitatively similar to that of a decrease in the beam yield-moment.

#### LIST OF REFERENCES

- 1. Hills, R. E., "Inelastic Behavior of Beams Subjected to Moving Loads," M.S. Thesis, Civil Engineering Department, Michigan State University, 1965.
- Newmark, N. M., "A Method of Computation for Structural Dynamics," Transaction, ASCE, Vol. 127, Part I, 1962, p. 1406.
- 3. Wen, R. K., Hills, R. E., and Toridis, T. G., "Elasto-Inelastic Beams Traversed by Massive Loads," Engineering Mechanics Division Specialty Conference, ASCE, Washington, D.C., October 12-14, 1966.
- 4. Wen, R. K., and Toridis, T. G., "Discrete Dynamic Models for Elasto-Inelastic Beams," Journal of the Engineering Mechanics Division, ASCE, Vol. 90, No. EM5, Proc. Paper 4081, October, 1964, pp. 71-102.
- 5. Toridis, T. G., and Wen, R. K., "Inelastic Response of Beams to Moving Loads," Journal of the Engineering Mechanics Division, ASCE, Vol. 92, No. EM6, Proc. Paper 5028, December, 1966, pp. 43-62.

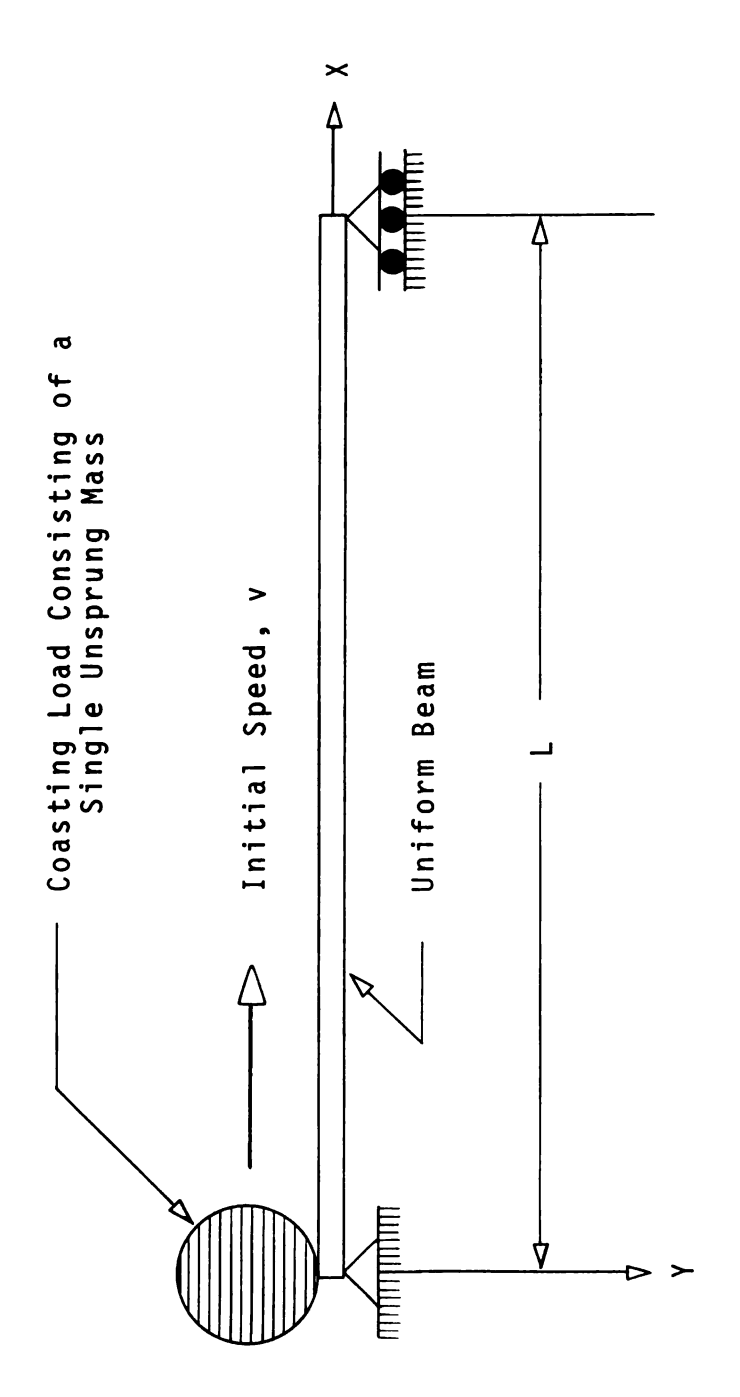


Figure 1. Initial State of Beam-Load System

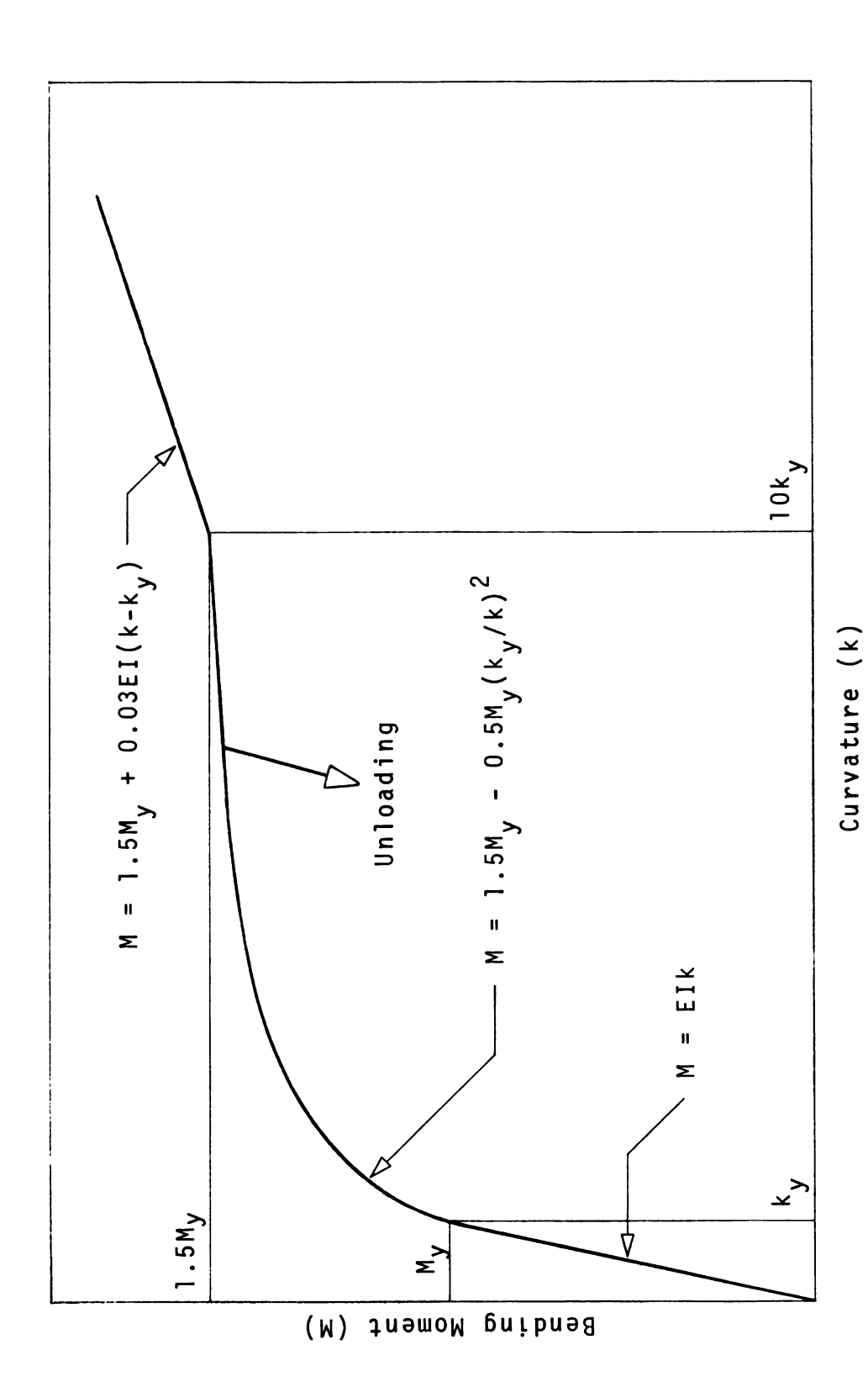


Figure 2. Moment-Curvature Diagram

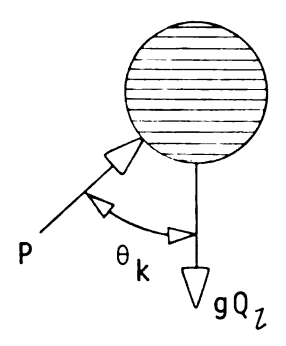


Figure 3a. Free Body Diagram of Moving Mass

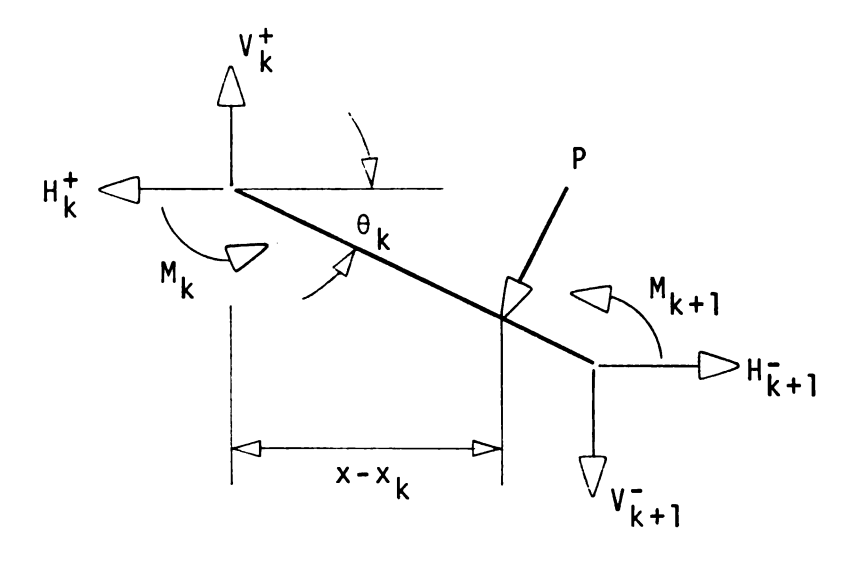


Figure 3b. Free Body Diagram of Panel (k)

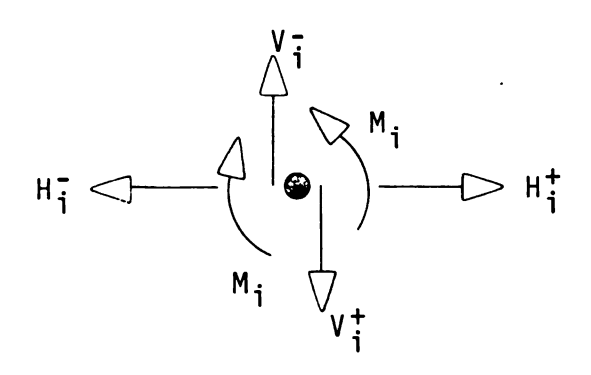


Figure 3c. Free Body Diagram of joint (i)

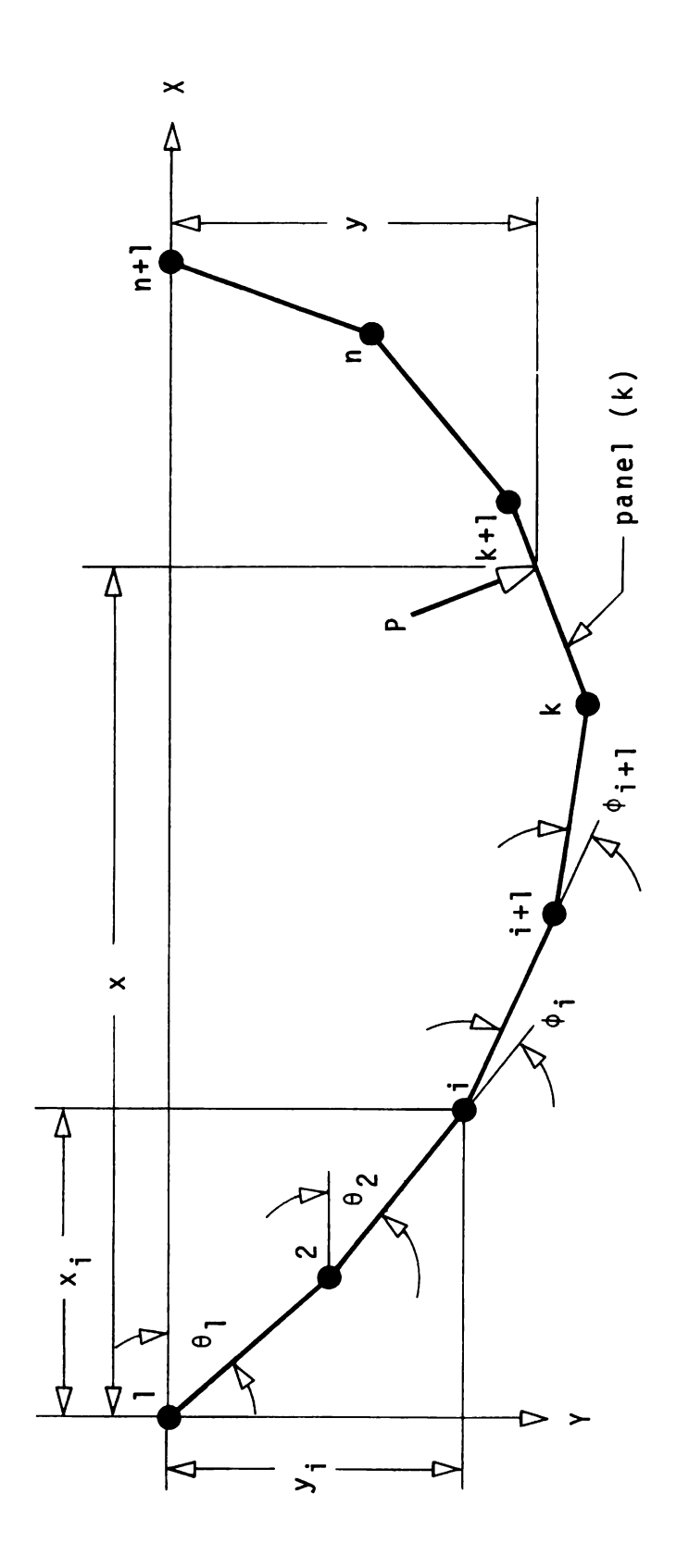
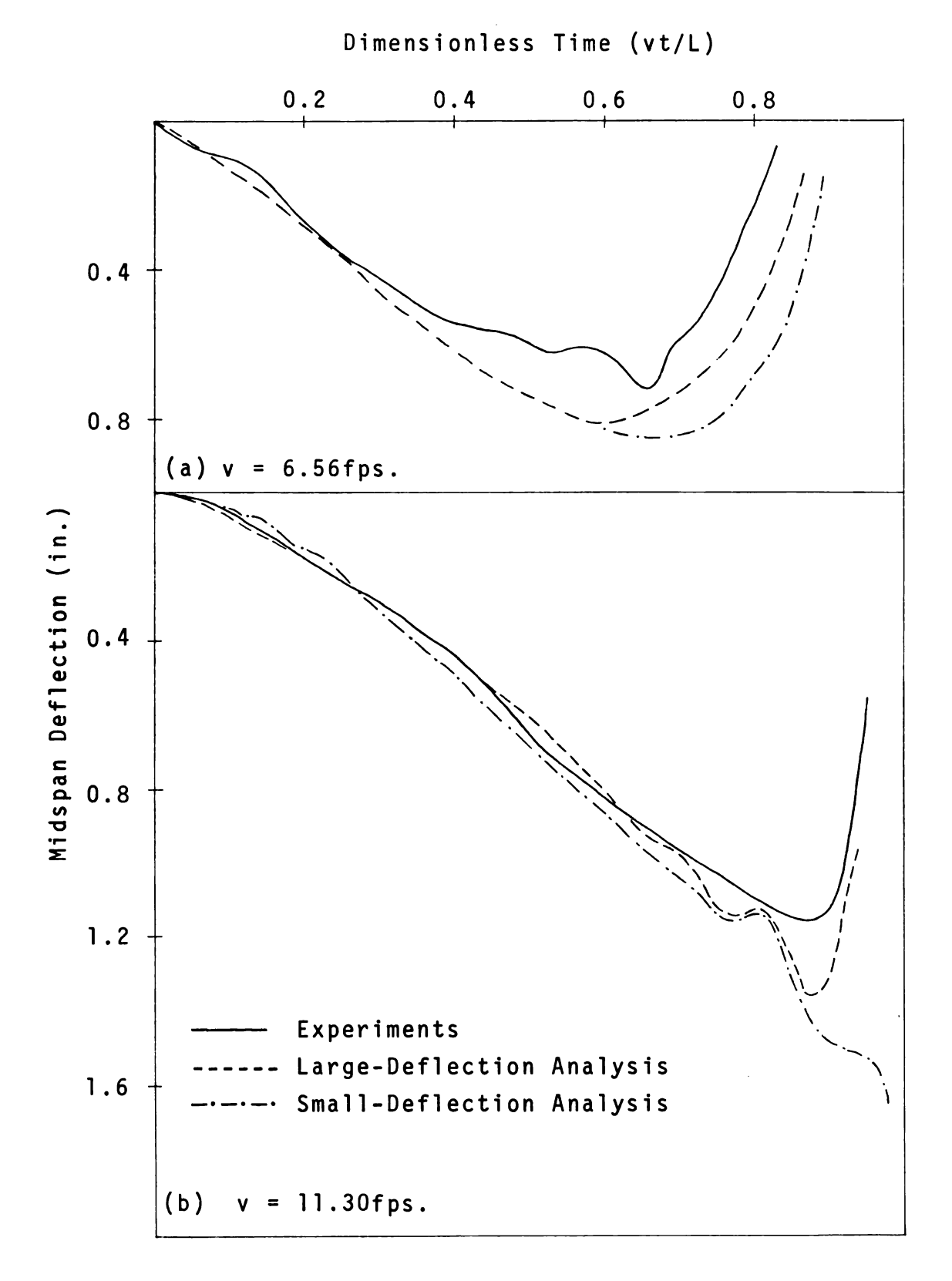


Figure 4. Discrete Model



Figures 5a, b. Midspan Deflection vs. Time

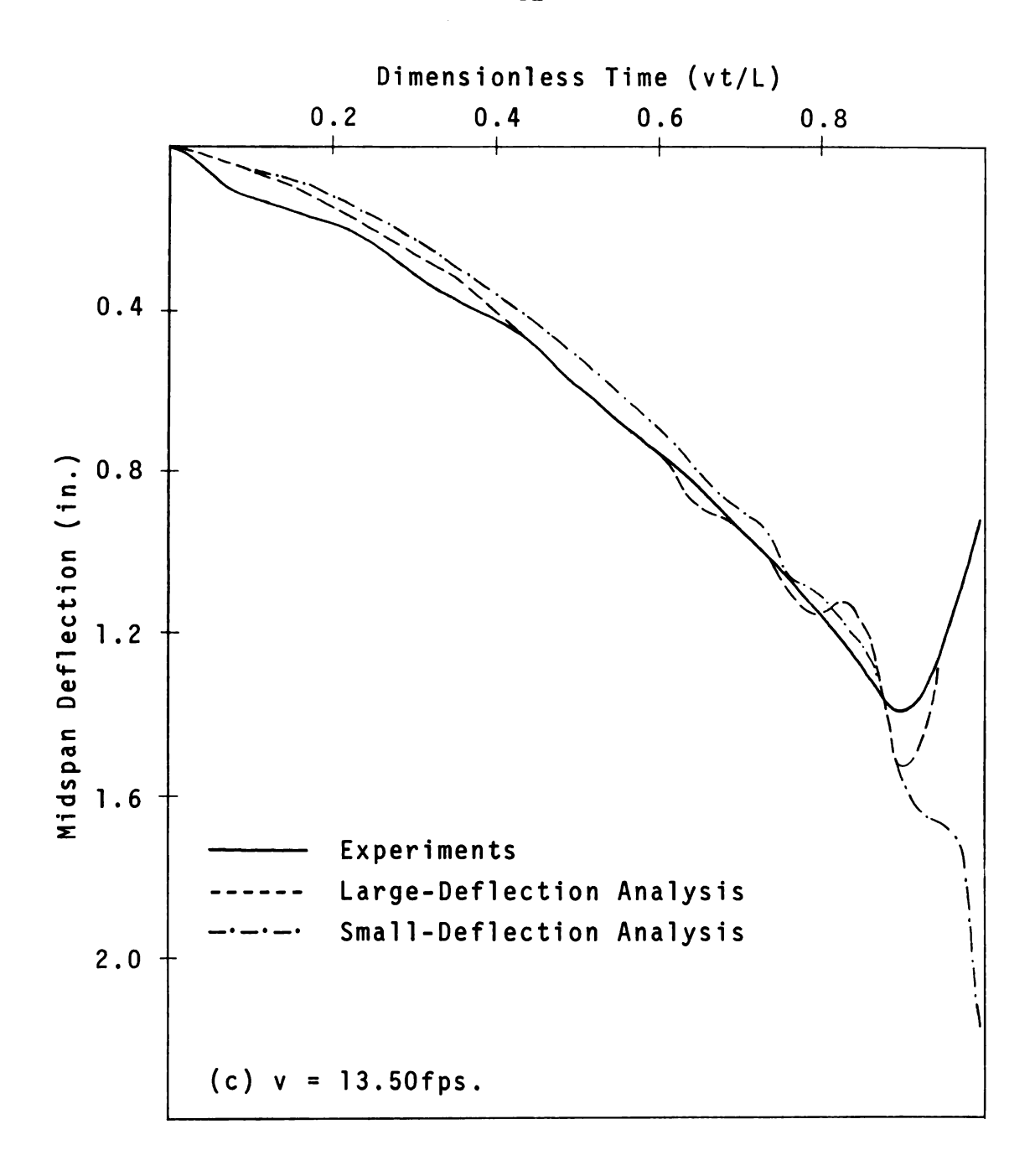


Figure 5c. Midspan Deflection vs. Time

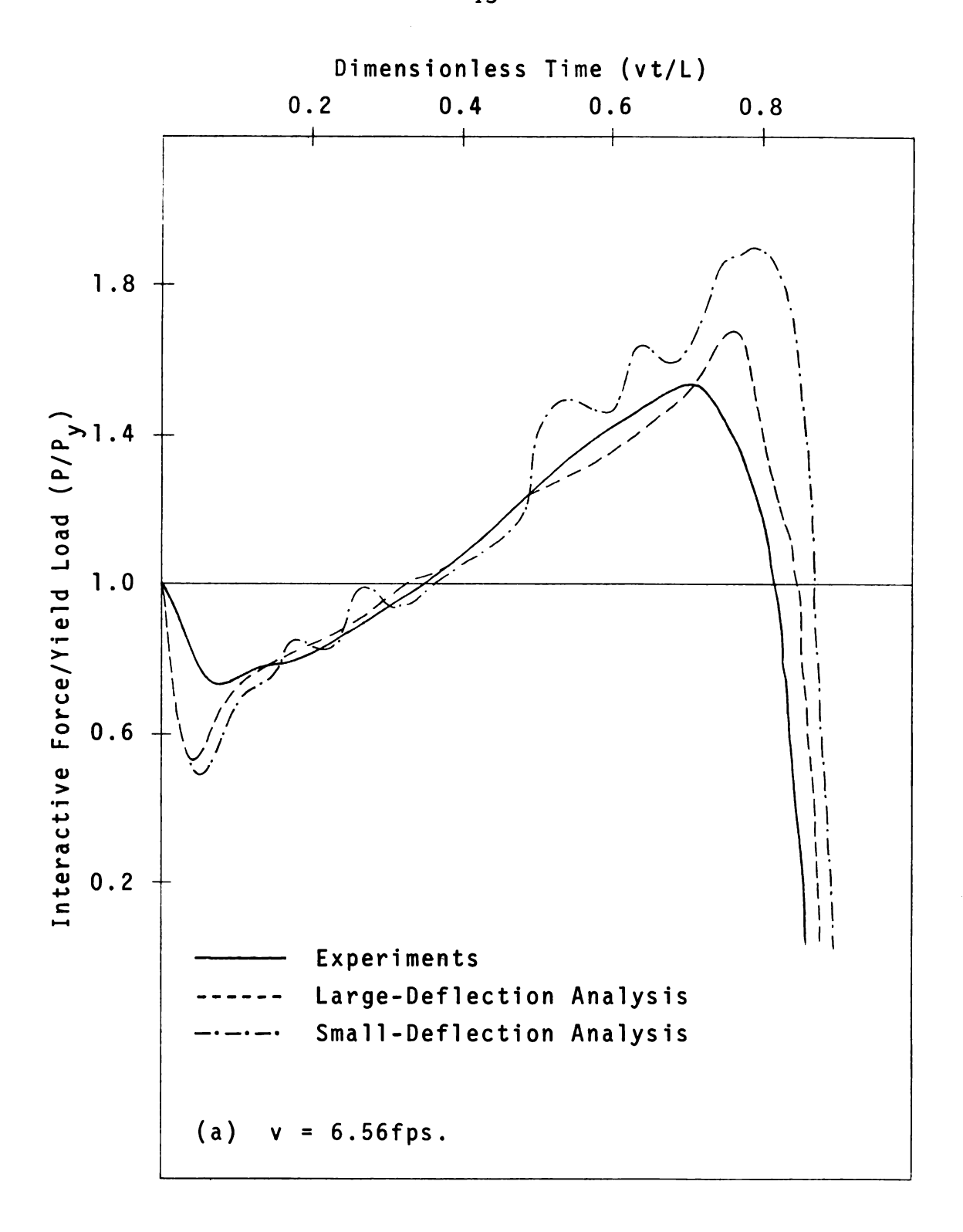


Figure 6a. Interactive Force vs. Time

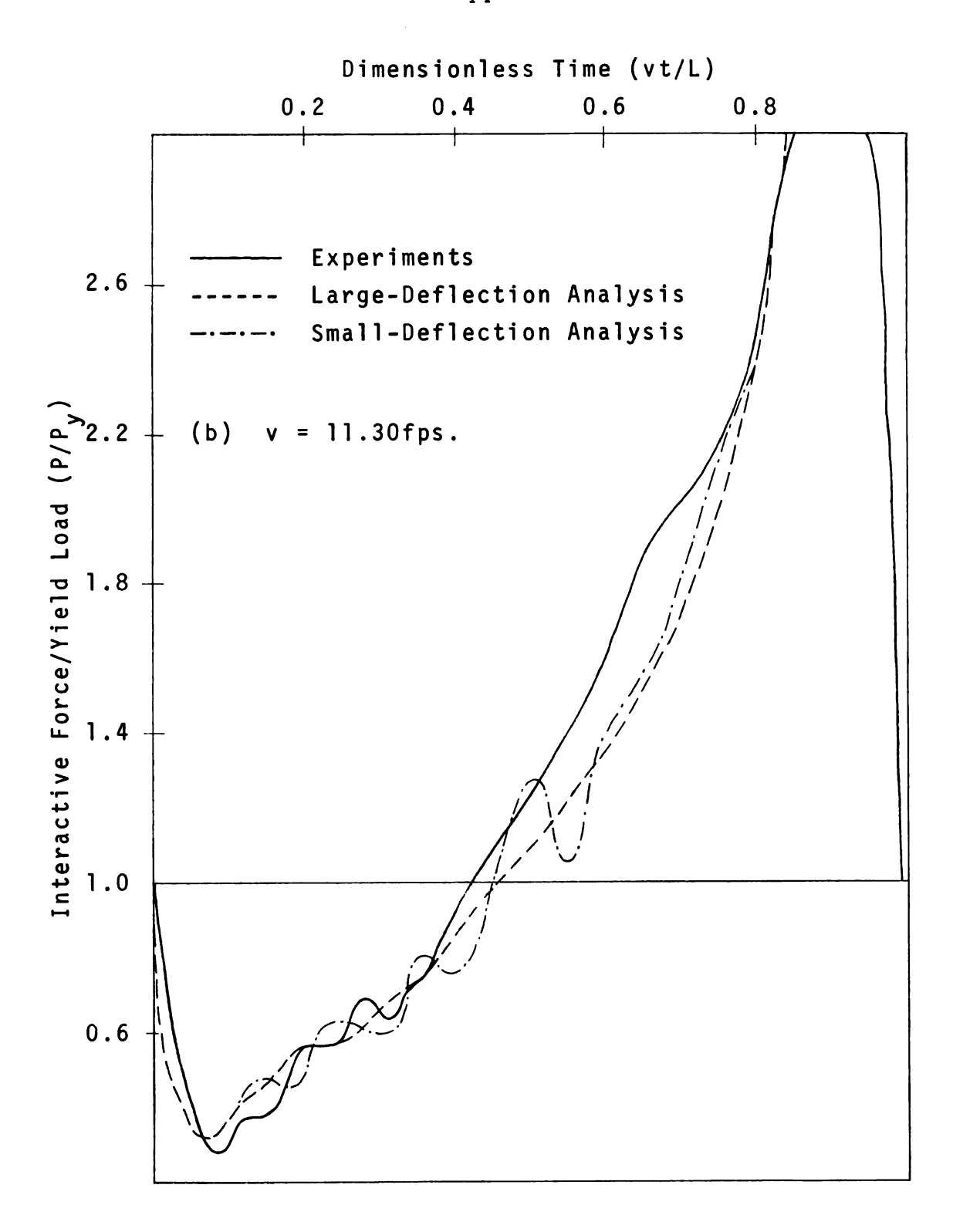


Figure 6b. Interactive Force vs. Time

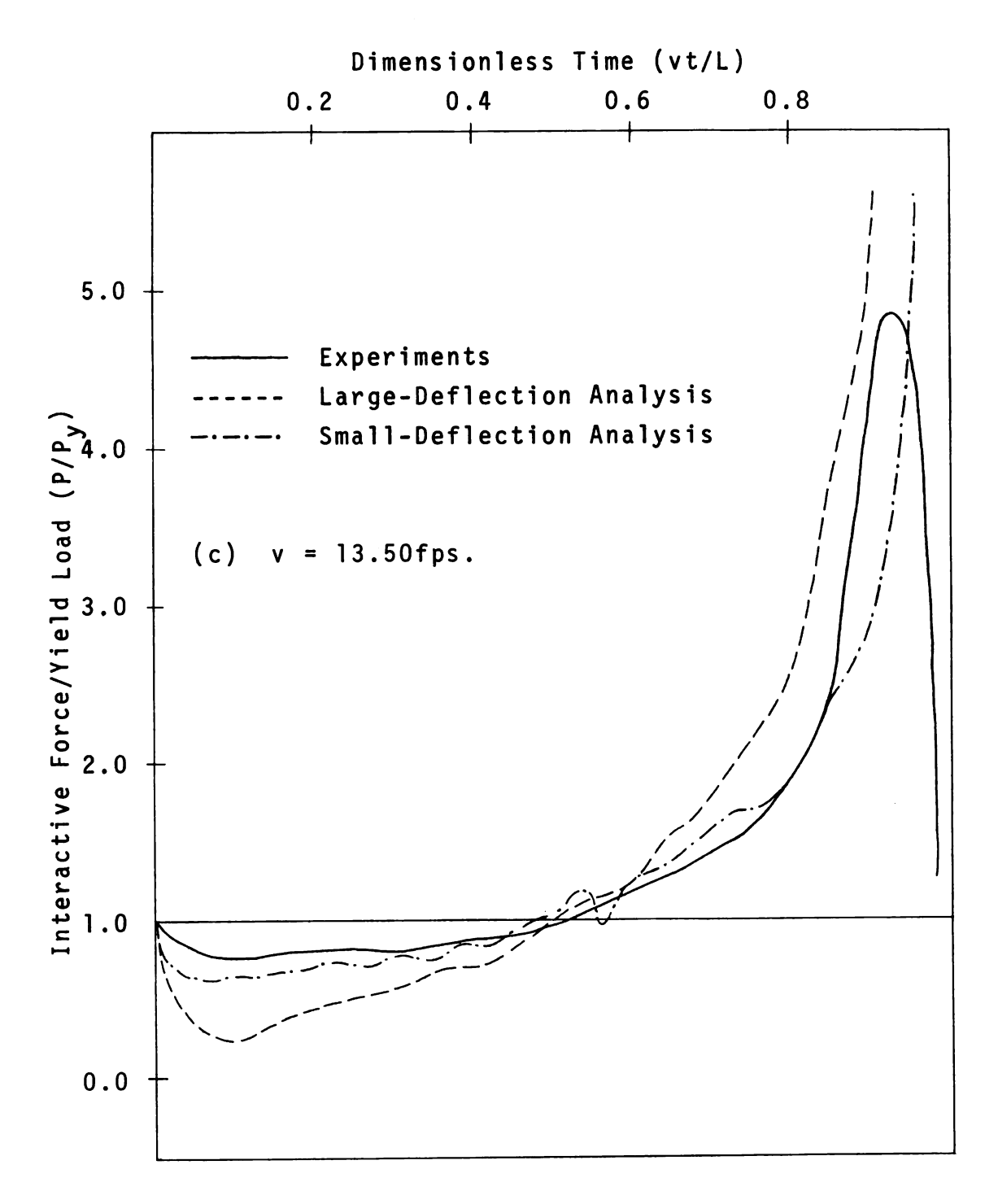


Figure 6c. Interactive Force vs. Time



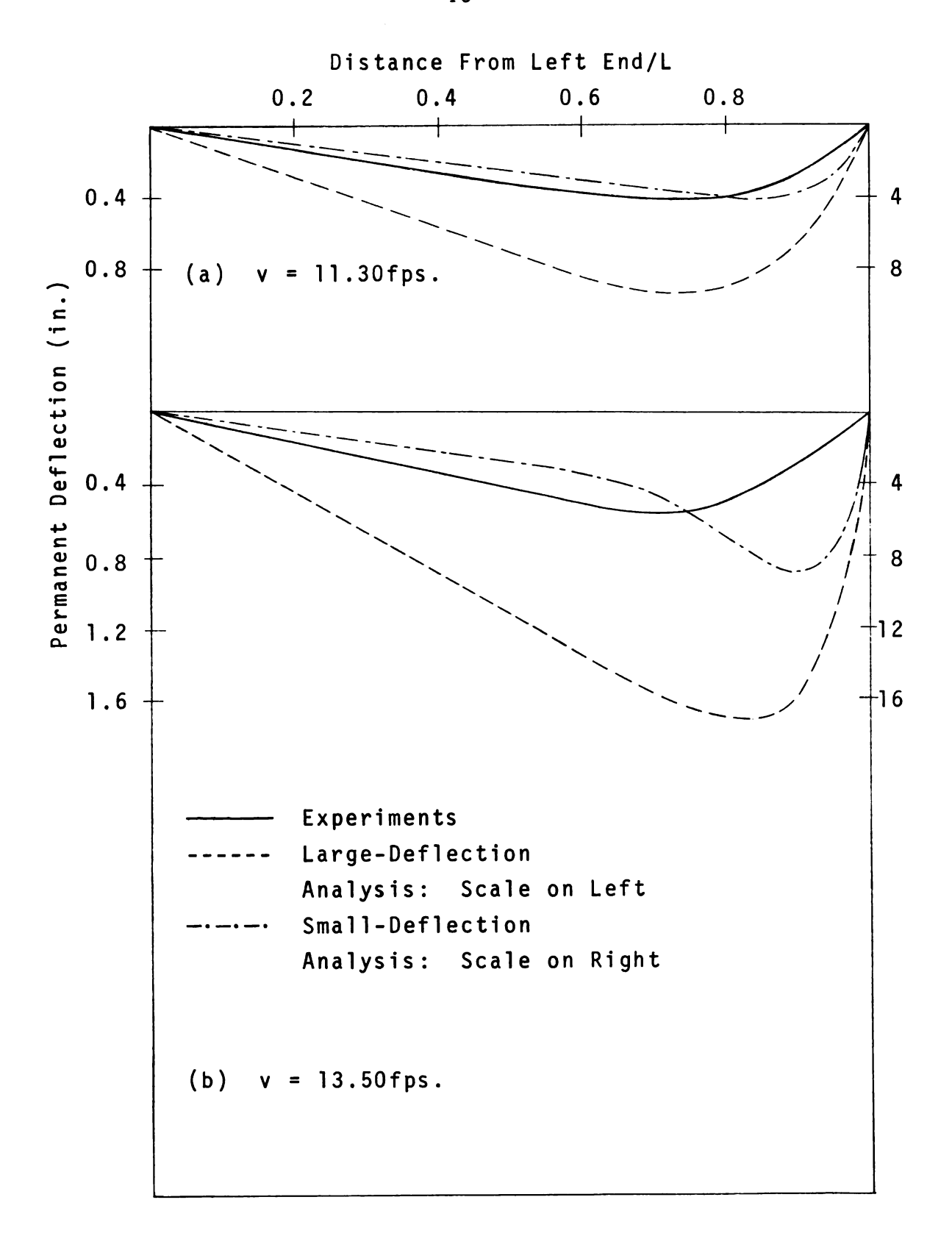
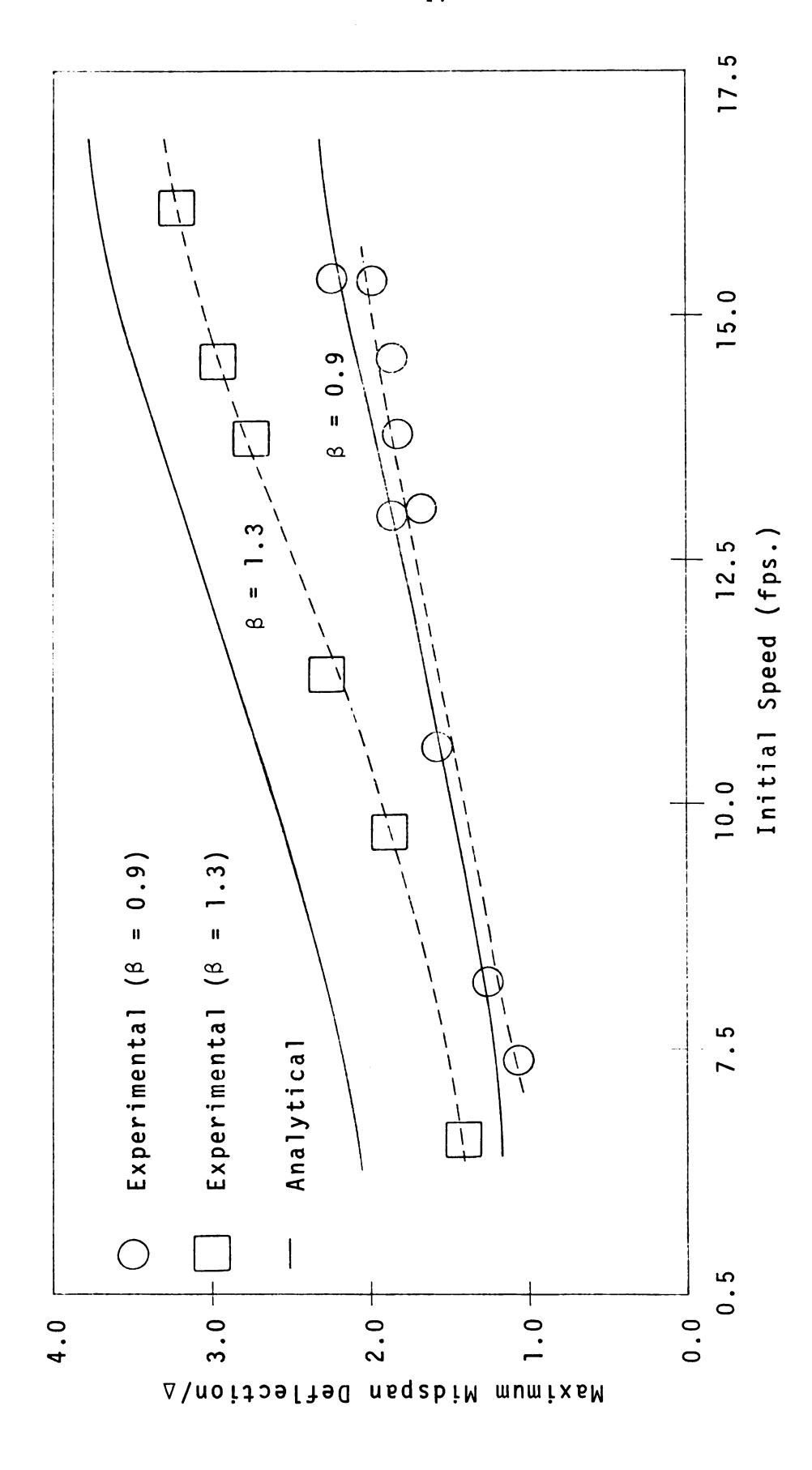
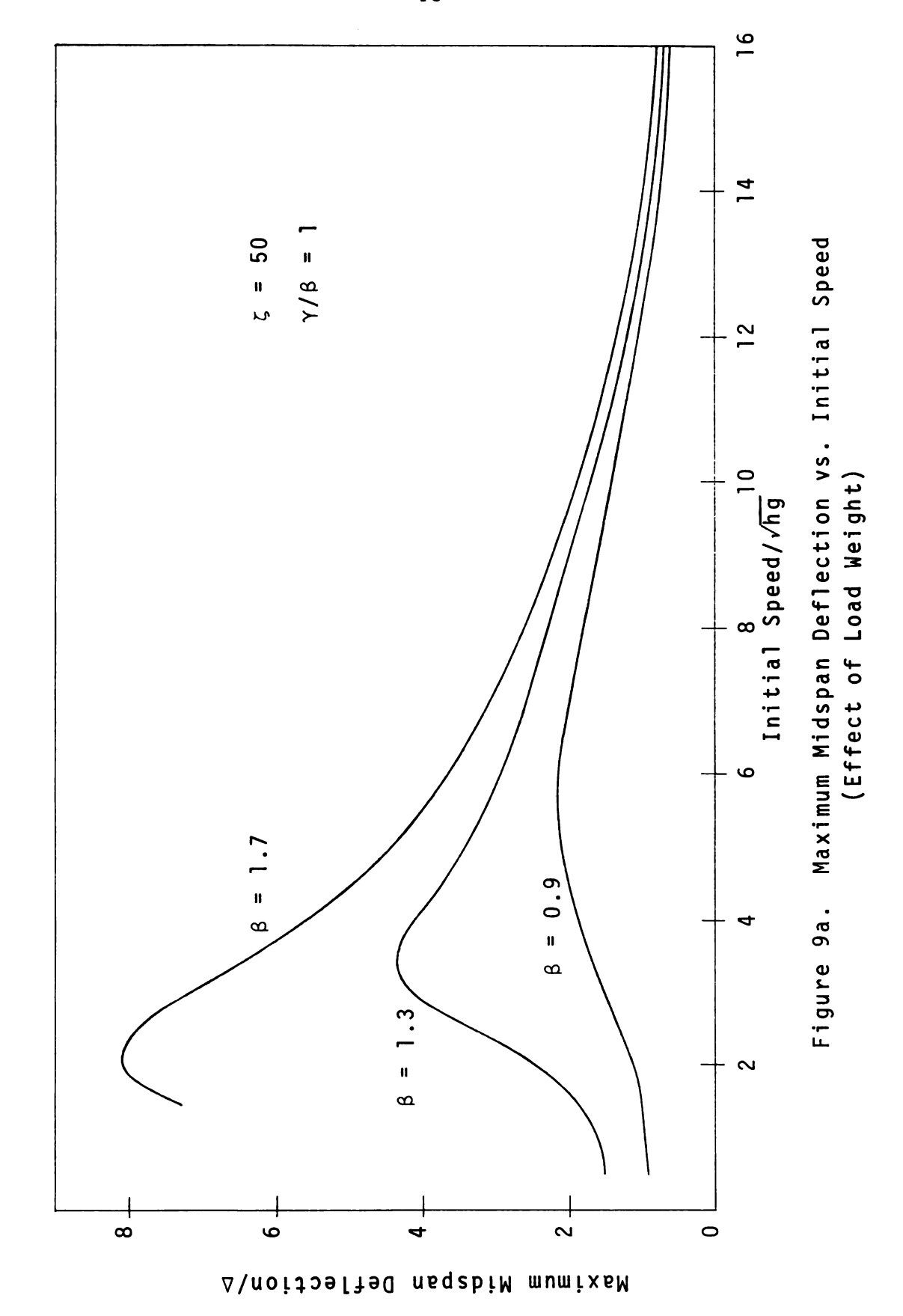
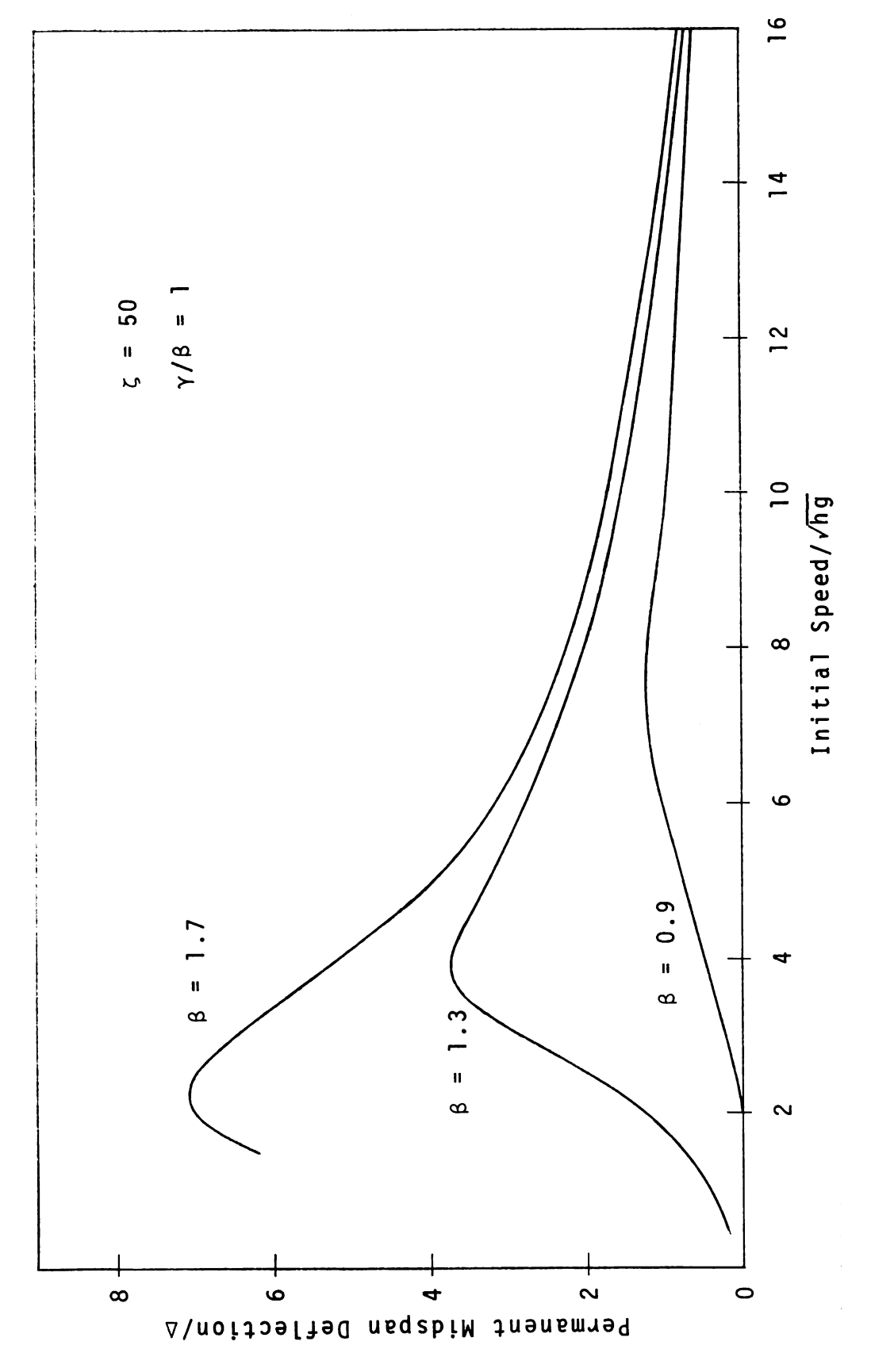


Figure 7. Permanent Sets

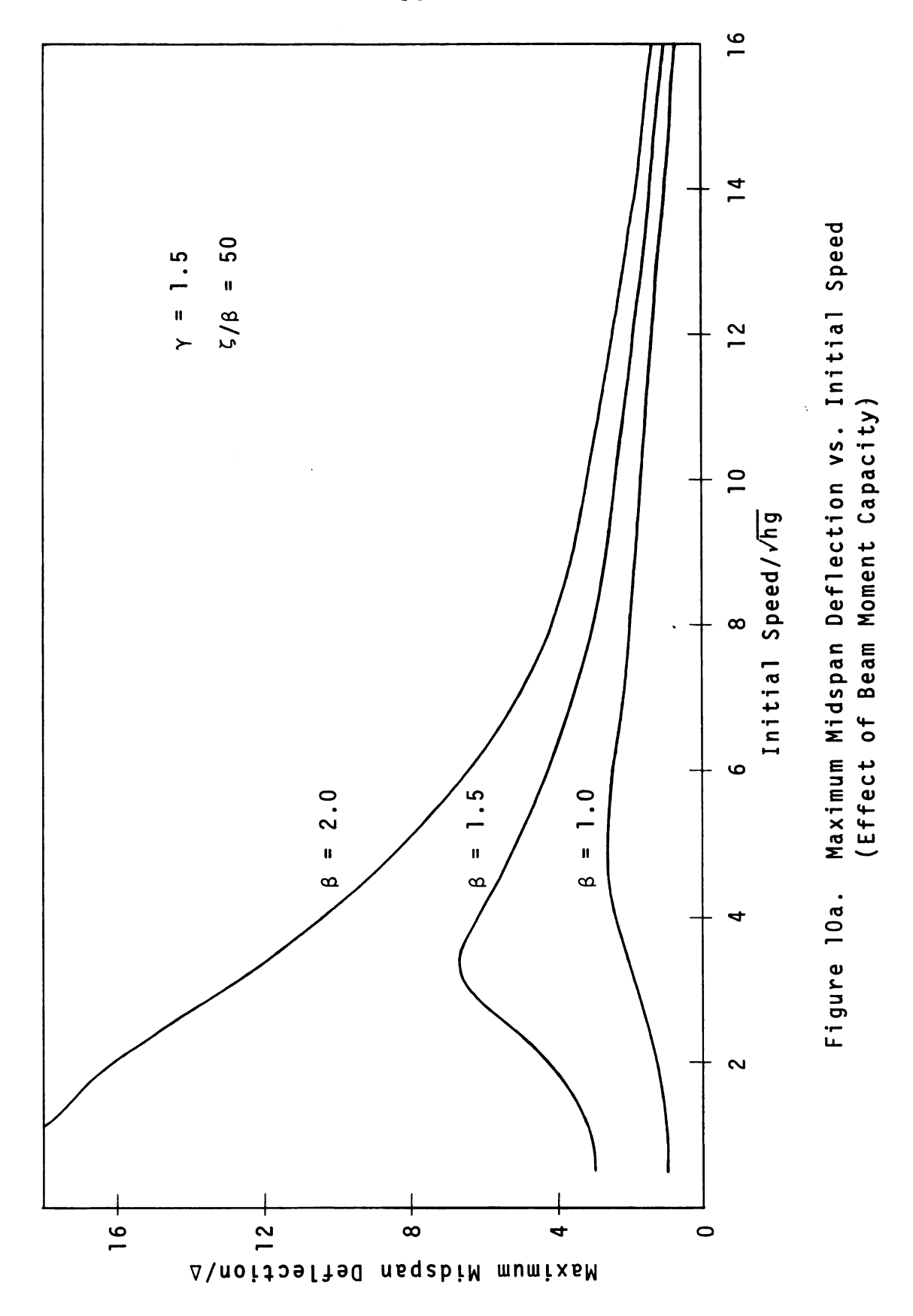


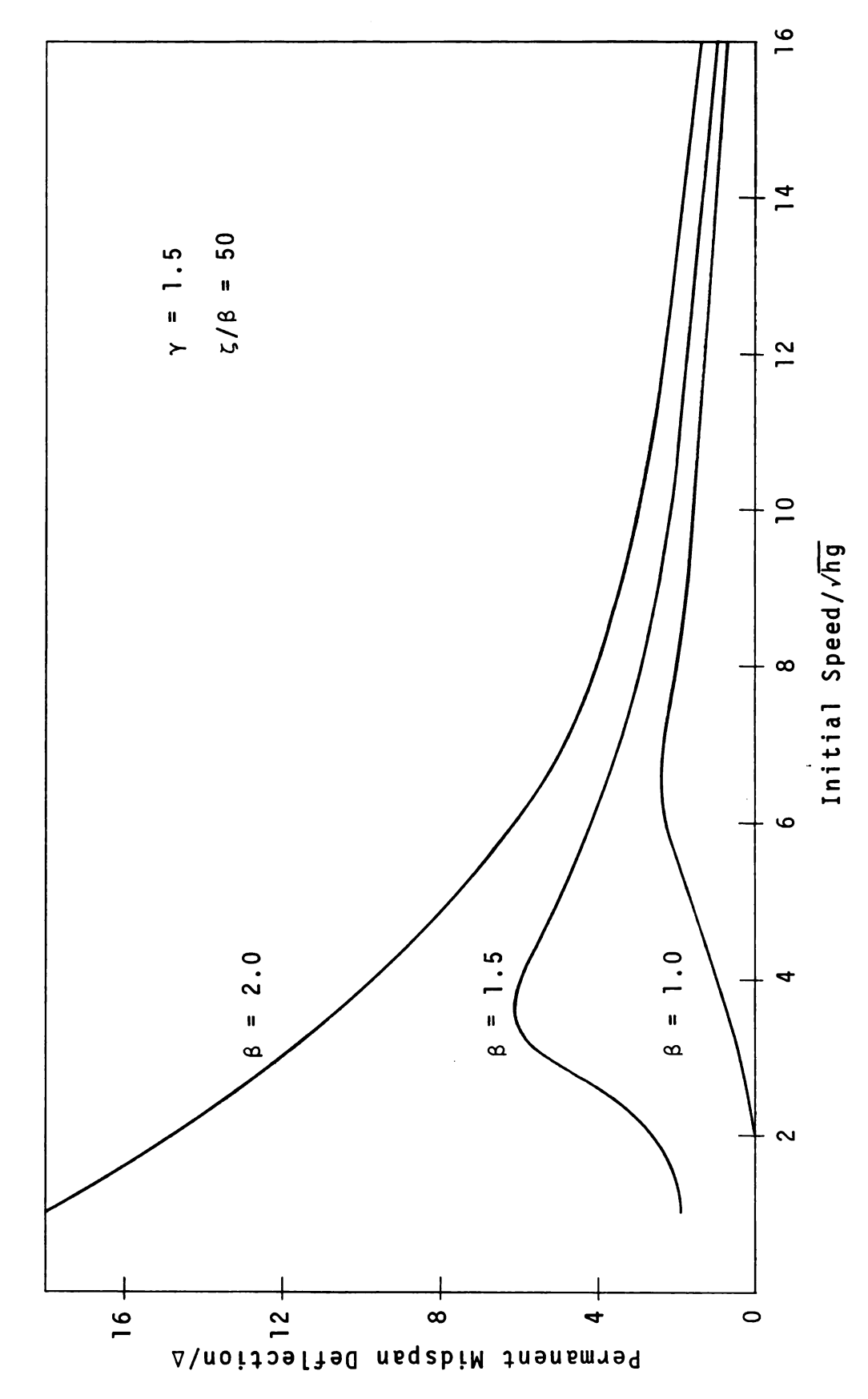
Maximum Midspan Deflection vs. Initial Speed (Analytical and Experimental) Figure 8.





Permanent Midspan Deflection vs. Initial Speed (Effect of Load Weight) Figure 9b.





Permanent Midspan Deflection vs. Initial Speed (Effect of Beam Moment Capacity) Figure 10b.

#### APPENDIX

#### COMPUTER PROGRAM

In this Appendix, the computer program as well as certain pertinent information are presented.

# 1. Identification of Parameters and Variables

The parameters and some important variables are identified in the following:

> Ν = n

ALPHA

BETA

GAMMA

ZETA = ζ

 $DELTA = \Delta/L$ 

= number of steps between two con-NS

secutive print-outs

DTIME  $= d\bar{t}$ 

= tolerance of iterations TOL

K

Z

 $= \bar{x} - \bar{x}_k$   $= k + (\bar{x} - \bar{x}_k)/\cos \theta_k$ S

Т

			_
D		_	כד
_		_	

$$H(I) = \overline{H}_{i}$$

TH(I) = 
$$\theta_{i}$$

AN1(I) = 
$$\phi_i$$

$$BMA(I) = \overline{M}_{i}$$

$$AX1 = \ddot{\ddot{x}}$$

$$\begin{array}{rcl}
\mathbf{VX1} & = & \mathbf{\dot{\bar{x}}} \\
\mathbf{DX1} & = & \mathbf{\bar{x}}
\end{array}$$

$$DX1 = \bar{x}$$

$$AX(I) = \ddot{x}_{i}$$

$$VX(I) = \dot{\bar{x}}_{i}$$

$$AYI(I) = \ddot{y}_{i}$$

$$VYl(I) = \dot{\bar{y}}_{i}$$

$$DY1(I) = \bar{y}_{i}$$

$$DYD(I) = y_i/\Delta$$

 $DYMAX(I) = maximum y_i/\Delta$ 

SDYMA(I) = S where  $y_i/\Delta$  attains its maximum

TDYMA(I) = T when  $y_i/\Delta$  attains its maximum

= maximum  $\overline{P}$ PMAX

= S where  $\overline{P}$  attains its maximum SPMA

TPMA = T when  $\overline{P}$  attains its maximum

 $PA(I) = permanent \phi_i$ 

PD(I) = permanent  $y_i/\Delta$ 

# 2. Print-outs

At the beginning, all the parameters as well as DELTA, NS, DTIME, and TOL are printed out.

During the process of step-by-step solution, S, DXl, VXl, AXl, P, T, and DYD(I) are also printed out.

At the end are printed out DYMAX(I), SDYMA(I), TDYMA(I), PA(I), PD(I), PMAX, SPMA, and TPMA.

#### COMPUTER PROGRAM

```
DIMENSION
                     AX(25), VX(25), AY1(25), AY2(25), AY3(25), VY1(25), VY2(25),
      1DY1(25),DY2(25),DYD(25),STGA(25),STGB(25),BMA(25),BMB(25),BMC(25),
      2BMU(25) •BML(25) •AN1(25) •AN2(25) •ANG(25) •PATH(25) •THPL(25) •CMB(25) •
      3CMT(25), CAB(25), CAG(25), PREM(25), PREA(25), PA(25), PD(25), DYMAX(25),
      4SDYMA(25),TDYMA(25),TH(25),DA(25),H(25),A(25),B(25)
C
C *** PARAMETERS ***
       N=
       ALPHA=
       BETA=
       GAMMA=
       7FTA=
C *** AUXILIARY VARIABLES ***
       N1 = N + 1
       DELTA=N/(12.0*ZETA)
       D=DELTA*N
      E=GAMMA*N
      F=E/ALPHA
       G=F*N/4.0
       TOL=1.0E-3
       DTIME=0.16/SQRT(G*ZETA)
       I=1.0E+3*DTIME+0.5
       DTIME=1.0E-3*1
       NS=5.0E-1/DTIME
       PPINT 602.N, ALPHA, BETA, GAMMA, ZETA, DELTA, NS, DTIME, TOL
  602 \text{ FORMAT}(1H1 \cdot 2(/) \cdot 4H \text{ N = I3} \cdot 9X \cdot 7HALPHA = F6 \cdot 2 \cdot 6X \cdot 6HBETA =
      1F5.2.5 \times 7HGAMMA = F6.2.5 \times 6HZETA = F6.2.5 \times 7HDELTA =
     2F7.4./.5H NS = I3. 8X.7HDTIME = F6.3. 6X.5HTOL = E8.1.2(/))
C
C *** INITIALIZATION OF VARIABLES ***
       ASSIGN 426 TO NAP
       K=L=0=VX1=1.0
       T=DX1=AX1=AX2=PMAX=0
       DO 600 I=1.N1
       AY1(I) = AY2(I) = AY3(I) = VY1(I) = VY2(I) = DY1(I) = DY2(I) = DYMAX(I) = 0
       BMA(I)=BMB(I)=BMC(I)=AN1(I)=AN2(I)=ANG(I)=PREM(I)=PREA(I)=0
       CAB(I) = CAG(I) = CMB(I) = CMT(I) = PD(I) = O
       STGA(I) = STGB(I) = 1.0
       BMU(I)=+1.0
```

```
600 BML(I)=-1.0
С
C *** RETURN ***
  604 M=NS
  608 DT=DTIME
C *** LOCATION OF COASTING LOAD ***
  300 DO 298 I=1.N
      DY2(I+1)=DY1(I+1)+DT*VY1(I+1)+0.5*DT**2*AY1(I+1)
  298 TH(I)=ASINF(DY2(I+1)-DY2(I))
      IF(K.EQ.0) GO TO 292
      DX2=DX1+DT*VX1+0.5*DT**2*AX1
      X=0
      DO 297 I=1.K
  297 \times X = X + COSF(TH(I))
      IF(L.EQ.0) GO TO 295
      IF(DX2-X) 294,295,296
  296 DT=(-VX1+SQRT(VX1**2-2*AX1*(DX1-X)))/AX1
      L=0
      GO TO 300
  295 Z=COSF(TH(K))
      ASSIGN 422 TO NAP
      L=1
      GO TO 293
  294 Z = DX2 - (X - COSF(TH(K)))
  293 S=K+(DX2-X)/COSF(TH(K))
  292 CONTINUE
С
C *** ANGLE OF ROTATION ***
      DO 18 I=2.N
      AN2(I)=TH(I-1)-TH(I)
   18 DA(I) = AN2(I) - AN1(I)
C
C *** BENDING MOMENT ***
      DO 240 I=2.N
      IF(1.5-STGA(I)) 200,200,201
C *** STAGE ONE ***
  201 BMB(I)=BMA(I)+DA(I)*ZETA
      IF(BML(I)-BMU(I)) 502,502,503
  503 IF(DA(I))
                500,500,501
  501 IF(BMB(I)-BML(I)) 240,240,271
  500 IF(BMB(I)-BMU(I)) 231,240,240
  231 CMB(I)=PREM(I)
      CAB(I)=PREA(I)
      STGB(I) = 2.1
      GO TO 222
  502 IF (DA(I)) 235,236,236
  235 IF(BMB(I)-BML(I)) 271,240,240
  271 \text{ STGB}(I) = 2.3
```

```
PREM(I) = CMT(I)
      PREA(I) = CAG(I)
      GO TO 222
  236 IF(BMB(I)-BMU(I)) 240,240,231
C *** STAGE TWO ***
  200 IF(DA(I)*PATH(I)) 221,222,222
  221 BMU(I)=BMA(I)
      STGB(I)=1.0
      BML(I)=BMU(I)+SIGNF(2.0.DA(I))
      CMB(I) = 0.5*(BMU(I) + BML(I))
      CAB(I) = AN1(I) + SIGNF(1.0.DA(I))/ZETA
      GO TO 201
  222 ANG(I)=AN2(I)-CAB(I)
      BMC(I)=FN(ZETA,ANG(I))
      BMB(I) = CMB(I) + BMC(I)
  240 CONTINUE
C
C *** AUXILIARY VARIABLES ***
      DO 20 1=2.N
   2^{\circ} B(I)=G*((BMB(I+1)-BMB(I))/COSF(TH(I))-
     1(BMB(I)-BMB(I-1))/COSF(TH(I-1))
   A^{O} X=Z/COSF(TH(K))**2
      A1=F*X
      A2=F*(SINF(TH(K))*TANF(TH(K-1))+COSF(TH(K)))-A1
      B1 = ALPHA * (X-COSF(TH(K)))
      B2=-ALPHA*X
      CC=1.0-A1*B2-A2*B1
C
C *** INTEGRATION BY BETA METHOD ***
 1000 DO 16 I=2.N
      AY2(I)=AY3(I)
   16 VY2(I)=VY1(I)+0.5*DT*(AY2(I)+AY1(I))
      VX2=VX1+0.5*DT*(AX2+AX1)
C *** VX(I) AND AX(I) ***
      DO 14 I=2.N1
      VX(I)=0
      AX(I)=0
      DO 14 J=2.1
      VX(I) = VX(I) - (VY2(J) - VY2(J-1)) *TANF(TH(J-1))
   14 AX(I)=AX(I)-(AY2(J)-AY2(J-1))*TANF(TH(J-1))-
     1(VY2(J)-VY2(J-1))**2/COSF(TH(J-1))**3
С
C *** H(I) ***
      H(N+1) = -0.5*AX(N+1)
      DO 12 I=2.N
      H(I)=H(N+1)
      DO 12 J=I+N
   12 H(I)=H(I)-Ax(J)
```

```
С
C *** AY3(K) AND AY3(K+1) ***
      DO 22 I=2.N
   22 A(I)=B(I)+H(I+1)*TANF(TH(I))-H(I)*TANF(TH(I-1))
      B3=BETA*COSF(TH(K))+ALPHA*AX(K)*SINF(TH(K))-
     12*ALPHA*(VX2-VX(K))*(VY2(K+1)-VY2(K))/COSF(TH(K))**2-
     23*ALPHA*Z*(VY2(K+1)~VY2(K))**2*TANF(TH(K))/COSF(TH(K))**3
      C = (B1*A(K)+B2*A(K+1)+B3)/CC
      IF(K.EQ.1) GO TO 44
      IF (K.EQ.N) GO TO 42
      AY3(K)=A(K)+A2*C
      AY3(K+1) = A(K+1) + A1 * C
      GO TO 46
   42 AY3(K) = (A(K)+A2*B3)/(1.0-A2*B1)
      GO TO 46
   44 AY3(K+1)=(A(K+1)+A1*B3)/(1.0-A1*B2)
   46 CONTINUE
C
C *** AY3(I) ***
      DO 66 I=2.N
      GO TO (62,66,66,64),I-K+2
   62 A3=-F*SINF(TH(K))*(TANF(TH(I))-TANF(TH(I-1)))
      AY3(I)=A(I)+A3*C
      GO TO 66
   64 AY3(I)=A(I)
   66 CONTINUE
C
C *** CHECK OF CONVERGENCE ***
      DO 68 I=2.N
      IF(ABSF(AY2(I)-AY3(I)).GT.TOL) GO TO 1000
   68 CONTINUE
C
C *** P AND AX2 ***
      P=B1*AY3(K)+B2*AY3(K+1)+B3
      AX2=P*SINF(TH(K))/ALPHA
      IF(P.GT.O) GO TO 480
      Q = 0
      M = 1
  480 CONTINUE
C
C *** JUMPS ***
      GO TO NAP
  422 ASSIGN 426 TO NAP
      VY=(VX2-VX(K))*TANF(TH(K))+
     1Z*(VY2(K+1)-VY2(K))/COSF(TH(K))**3+VY2(K)
      X = (1 \cdot 0 + E) * (1 \cdot 0 + TANF(TH(K)) * TANF(TH(K+1)))/E
      DVY = (VY - VY2(K+1) - (VX2 - VX(K+1)) * TANF(TH(K+1)))/X
      VY1(K+1)=VY2(K+1)=VY2(K+1)+DVY
      VX1=VX2=VX2+DVY*TANF(TH(K))/E
```

```
T = T + DT
      DT=Z=0
      K=K+1
      IF(K.LE.N) GO TO 80
      Q = 0
      M = 1
  426 CONTINUE
С
C *** INITIAL CONDITIONS FOR NEXT STEP OF SOLUTION ***
      T=T+DT
      DX1 = DX2
      VX1 = VX2
      AX1 = AX2
      DO 45 I=2.N
      PATH(I) = BMB(I) - BMA(I)
      BMA(I) = BMB(I)
      DY1(I)=DY2(I)
      VY1(I)=VY2(I)
      AY1(I) = AY3(I)
      AN1(I) = AN2(I)
      CMT(I) = CMB(I)
      CAG(I) = CAB(I)
      STGA(I)=STGB(I)
      DYD(I) = DY1(I)/D
   45 CONTINUE
С
C *** MAXIMUM RESPONSE ***
      IF(K.EQ.0) GO TO 408
      DO 404 1=2.N
      IF(DYMAX(I).GE.DYD(I)) GO TO 404
      DYMAX(I)=DYD(I)
      SDYMA(I)=S
      TDYMA(I)=T
  404 CONTINUE
      IF(PMAX.GE.P) GO TO 408
      PMAX=P
      SPMA=S
      TPMA=T
  408 CONTINUE
C
C *** PRINT-OUTS ***
      IF(M.GT.O) GO TO 608
      PRINT 442, S, DX1, VX1, AX1, P
  442 FORMAT(1H ,3HS =F5.2, 7x.5HDX1 =<math>F5.2.11X.5HVX1 =
     1F7.4,12X,5HAX1 = E9.2,10X,3HP = E9.2
      PRINT 446,T,(DYD(I),I=2,N)
  446 FORMAT(1H +3HT =F5.2+ 7X+8HDYD(1) =F5.2+8F12.2/(F29.2+8F12.2))
      IF(Q.GT.O) GO TO 604
```

```
PRINT 30
   30 FORMAT(3(/) **MAXIMUM RESPONSE*)
      PRINT 31 \cdot (DYMAX(I) \cdot I = 2 \cdot N)
   31 FOPMAT(*DYMAX(!) =*, 7X,9F12,2/(5X,10F12,2))
      PRINT 32 \cdot (SDYMA(I) \cdot I = 2 \cdot N)
   32 FORMAT(*SDYMA(I) =*, 7X,9F12.2/(5X,10F12.2))
      PRINT 33 (TDYMA(I) • I=2 • N)
   33 FORMAT(*TDYMA(]) =*, 7X,9F12.2/(5X,10F12.2))
C
C *** PERMANENT SET ***
      DO 23 I=2.N
   23 PA(I)=AN1(I)-BMA(I)/ZETA
      U=0
      X = 0
      Y = 0
      DO 24 I=2.N
      U=U+PA(I)
      X=X+SINF(U)
   24 Y=Y+COSF(U)
      PA(1) = ATANF(X/(1.0+Y))
      DO 25 I=3.N1
      U=0
      DO 25 J=3.I
      U=U+PA(J-1)
   25 PD(I) = PD(I) + SINF(PA(I) - U)
      DO 26 I=2.N1
   26 PD(1)=(SINF(PA(1))+PD(1))/D
      PRINT 37 \cdot (PA(I) \cdot I = 1 \cdot N)
                          =*,E11,2,9E12,2/(9X,10E12,2))
   37 FORMAT(*PA(I)
      PRINT 38 (PD(I) + I=1 + N1)
   38 FORMAT(*PD(I)
                          =* •E11 • 2 • 9E12 • 2/(9X • 10E12 • 2))
      PRINT 39, PMAX, SPMA, TPMA
   39 FORMAT(1(/),*PMAX =*,E12.5,10X,*SPMA =*,E12.5,10X,*TPMA*,E12.5)
      END
      FUNCTION FN(ZETA THETA)
      STHD=10.0
      FLEX=1.0/ZETA
      IF(ABSF(THETA).LE.STHD*FLEX) GO TO 750
      X=1.5+0.03*(ZETA*ABSF(THETA)-STHD)
      IF(THETA.LT.O) X=-X
      GO TO 770
  750 IF(ABSF(THETA).LE.FLEX) GO TO 760
      X=1.5-0.5/(ZETA*ABSF(THETA))**2
      IF(THETA.LT.O) X=-X
      GO TO 770
  760 X=ZETA*THETA
  770 FN=X
      END
```

MICHIGAN STATE UNIVERSITY LIBRARIES
3 1293 03056 3344